Real-Time EEG Response to Pulsed Transcranial Photobiomodulation in Healthy Young Adults: Effects of Stimulation Parameters, Skin Tone, and Sex

Alicia A. Mathew[1], Hannah Van Lankveld[1,2], Xiaole Z. Zhong[1,3], Joanna X. Chen[1,2] , Sophie Niculescu[1], Lew Lim[4], Reza Zomorrodi[4,5], and J. Jean Chen[1,2,3]

1 - Rotman Research Institute, Baycrest Health Sciences, Toronto, ON, Canada;
2 - Department of Biomedical Engineering, University of Toronto, Toronto, ON, Canada;
3 - Department of Medical Biophysics, University of Toronto, Toronto, ON, Canada;
4 - Vielight Inc., Toronto, ON, Canada;
5 - Temerty Centre for Therapeutic Brain Intervention, Center for Addiction and Mental Health, Toronto, ON, Canada

ABSTRACT

Transcranial photobiomodulation (tPBM) represents a promising non-invasive neuromodulation approach, yet how stimulation parameters interact with individual biological factors to determine neural outcomes remains unclear. This study provides the first analysis of parameter-dependent tPBM effects on real-time brain activity in 46 participants with diverse skin tones, quantified via individual topography angle (ITA). EEG was recorded before, during, and after right prefrontal cortex tPBM while participants watched naturalistic videos. Protocols were designed with two wavelengths (808/1064 nm), two pulsation frequencies (10/40 Hz), and three irradiances (100/150/200 mW/cm^2) to analyze baseline-normalized changes in EEG band power and sample entropy during and post-stimulation. Both wavelengths produced distinct spectral reorganization patterns with fundamentally different profiles. 808 nm achieved net delta reductions while enhancing alpha and gamma power, with 40 Hz producing the largest global alpha increases among all conditions. Conversely, 1064 nm increased delta power but generated larger beta and gamma enhancement at 40 Hz. Across wavelengths, 40-Hz stimulation produced greater low-to-high frequency power shifts compared to 10 Hz. Sample entropy changes remained stimulus-bound, while power effects persisted post-stimulation, particularly gamma with 808 nm and beta-gamma with 1064 nm at 40 Hz. Notably, biological factors profoundly modulated responses: lighter skin tones consistently showed enhanced effects across multiple frequency bands, while sex-dependent patterns emerged with males demonstrating distinct theta responses at 40 Hz. These multi-parameter interactions revealed complex effects that challenge simplified parameter selection approaches. The profound influence of skin tone and sex on treatment responses necessitates personalized protocols for equitable therapeutic outcomes, establishing EEG as a sensitive biomarker for precision neuromodulation across diverse demographics.

1 INTRODUCTION

Transcranial photobiomodulation (tPBM) represents a promising frontier in non-invasive neuromodulation, delivering red to near-infrared (NIR) light (600-1100 nm) through the scalp to boost mitochondrial metabolism and cortical function. By activating cytochrome c oxidase (CCO) and stimulating endothelial nitric oxide synthase (eNOS), tPBM contributes to increased adenosine triphosphate (ATP) production, enhanced vascular response, neuroprotection, and improved cerebrospinal fluid (CSF) outflow and production (Hamblin, 2018a; Hennessy & Hamblin, 2017; Motsenyat et al., 2025; Salehpour et al., 2018; Vargas et al., 2017; Yokomizo et al., 2022). These mechanisms translate to cognitive improvements across attention, reaction time, memory, and executive function in diverse age groups following both single and repeated tPBM sessions (Chan et al., 2019; Gonzalez-Lima & Barrett, 2014; Vargas et al., 2017). However, behavioral measures remain susceptible to practice effects and participant variability (Hess et al., 2020), highlighting the need for objective, real-time biomarkers of neural response.

Electroencephalography (EEG) is an ideal candidate for monitoring tPBM's neural effects, offering high temporal resolution for tracking changes across canonical frequency bands (delta, theta, alpha, beta, gamma) (Berger, 1929; Nunez & Srinivasan, 2005; Thut et al., 2012). Each band reflects specific neural states and pathological signatures that remain clinically relevant when controlling for attentional states (eyes open/closed, task engagement) and biological factors (sex, age) (Getzmann et al., 2024; Kang et al., 2024; Neuhaus et al., 2021). Normal aging, for instance, is associated with increased slow-wave (delta-theta) activity alongside slower alpha rhythms (R.E. Dustman, D.E. Shearer, Y. Emmerson, n.d.), theta and alpha power reductions (Barry & De Blasio, 2017; López-Loeza et al., 2016; Stacey et al., 2021), increased beta power ((Barry & De Blasio, 2017; Getzmann et al., 2024; Kang et al., 2024; Neuhaus et al., 2021); (Barry & De Blasio, 2017; Stacey et al., 2021), and higher gamma power (Jabès et al., 2021; López-Loeza et al., 2016). In contrast, Alzheimer's disease (AD) typically manifests as elevated delta-theta power with decreased alpha, beta, and gamma power (Adler et al., 2004; Babiloni et al., 2020; Jelic et al., 2000; Jeong, 2004). These consistent spectral signatures position EEG as a suitable tool for directly tracking tPBM's band-specific neuromodulatory effects.

Despite promising results from existing tPBM-EEG studies, critical gaps remain in understanding how stimulation parameters interact with biological factors to shape neural outcomes across diverse populations. Current evidence reveals some consistent patterns: gamma power increase appears particularly robust across multiple protocols, observed during continuous-wave 830-nm stimulation (Spera et al., 2021), 40-Hz pulsed 810-nm targeting of the default mode network (DMN) with intranasal delivery (Zomorrodi et al., 2019), and various wavelength-frequency combinations including 660-nm & 40-Hz, 660-nm & 100-Hz, and 850-nm & 40-Hz (Tang, Jiang, et al., 2023). Other frequency bands show parameter-dependent responses, with right prefrontal 1064-nm tPBM reducing delta power while improving response speed (Jahan et al., 2019), 40-Hz pulsed 810-nm elevating alpha power while reducing delta and theta (Zomorrodi et al., 2019), and time-resolved alpha and beta power increasing during 1064-nm stimulation (X. Wang et al., 2019a). However, biological factors represent the most prominent knowledge gap for optimal personalized treatment. Melanin's strong NIR absorption likely limits dose delivery in darker skin (Sandell & Zhu, 2011), a factor not yet tested in EEG studies despite profound implications for treatment equity. Similarly, sex dependencies in tPBM responses remain understudied and unclear. Understanding these interactions is further complicated by parameter relationships: simulations indicate that 808 nm delivers more energy to the cortex through lighter skin (Cassano et al., 2019; Li et al., 2017; Van Lankveld et al., 2024a), effective irradiances of 75-250 mW/cm^2 follow biphasic mitochondrial dose-responses (Henderson & Morries, 2015; Huang et al., 2011; X. Wang et al., 2016; Zein et al., 2018), and stimulus frequency may engage endogenous rhythms differently, with 10 Hz aligning with alpha oscillations while 40 Hz targeting gamma (Iaccarino et al., 2016; Zomorrodi et al., 2019).

To address these limitations, our study presents the first multi-parameter analysis of tPBM's real-time neural responses across 46 participants with diverse skin tones. We investigate the independent and interactive effects of wavelength (808/1064 nm), frequency (10/40 Hz), and irradiance (100/150/200 mW/cm^2) to provide insights into how parameter choice and biological factors shape tPBM outcomes. Our approach combines EEG band power analysis with sample entropy measures to capture both oscillatory strength and signal complexity to uncover a multidimensional picture of tPBM's neuromodulation, establishing a guideline for more optimized tPBM protocols.

2 METHODS

2.1 Participants and Skin Tone Measurements

Forty-six healthy young adults (20-32 years; 24M/22F) with diverse skin tones from the Baycrest Participants Database completed four EEG-tPBM scans each. Exclusion criteria included neurological or physiological disorders and substance use. Ethical approval was obtained from the Baycrest Research Ethics Board and all participants provided written informed consent. Forehead skin pigmentation was quantified via spectrophotometry (CM-600D, Konica Minolta, Tokyo, Japan), yielding CIE L^* b^* values to compute individual topography angles (ITA) with **Equation 1**:

$$ITA = arctan(\frac{L^*-50}{b^*}) \times \frac{180}{\pi} \quad (1)$$

Six readings were taken from an 8-mm area on the right forehead and averaged per participant. Higher ITAs indicate lighter skin tones, specifically lower levels of eumelanin, the main skin-tone chromophore. ITA was treated continuously in analyses but stratified into three groups to ensure balance.

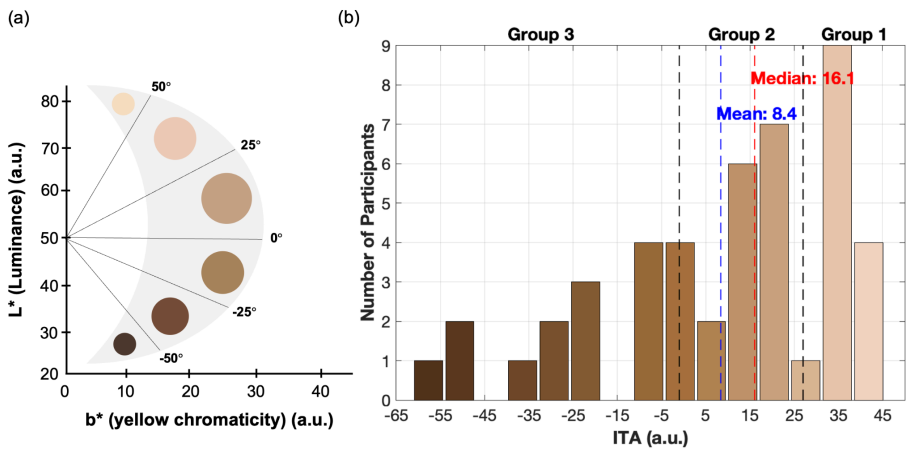

Figure 1. (a) ITA as a quantification of skin tone. (b) Participant distribution across ITAs (median ± range = 16.1 ± 106.7), with the mean and median in blue and red respectively, and group (Groups 1, 2, 3) boundaries in black.

2.2 tPBM Protocol

Stimulation targeted the right prefrontal cortex (rPFC) using MDL-III lasers at 808 nm or 1064 nm and light was delivered via 400 µm fiber to a custom headpiece (**Fig. 2a**) (Vielight Inc., Toronto, Canada). Each participant completed four scans with distinct combinations of wavelengths (808 nm or 1064 nm), pulsation frequencies (10 Hz or 40 Hz), and irradiances (100, 150, or 200 mW/cm^2). These parameters were selected as 808 nm and 1064 nm are widely used in tPBM studies due to their established tissue penetration and safety profiles, while 10 Hz and 40 Hz pulsation frequencies have demonstrated efficacy in prior studies. Parameters were remotely controlled and participants were blinded to the protocols and study design. Each 12-min scan followed a PRE-DURING-POST design (4 minutes each) where the baseline (PRE) period served as a within-subject control in the absence of a formal sham stimulation. Participants watched naturalistic stimulus videos to minimize drowsiness (Gal et al., 2022). No thermal sensations were reported. Three distinct protocols were designed using the above parameter combinations (**Table 1**). The number of participants per skin tone group per protocol was as balanced as possible. **Table 2** contains a detailed list of treatment parameters.

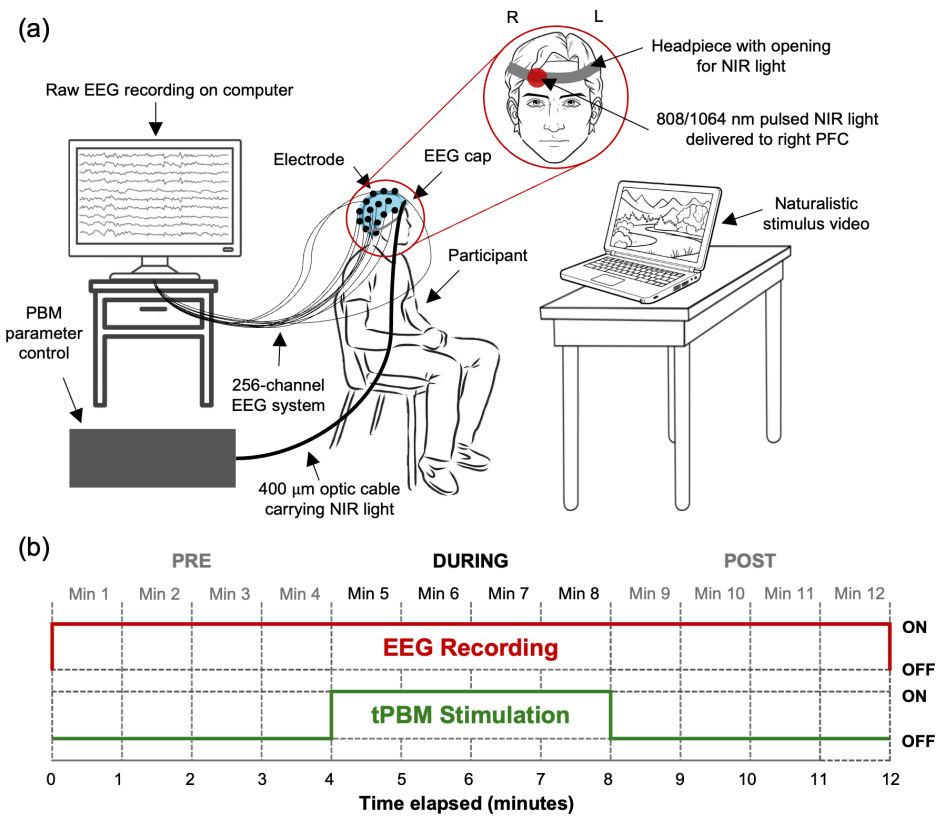

Figure 2. (a) Illustration of EEG-tPBM experimental setup. (b) Single EEG scan timeline following block design.

Table 1. Participant distribution by skin tone group and protocol with specific parameter combinations.

Skin Tone Group	ITA Range	Protocol 1	Protocol 2	Protocol 3	Total	M/F
Group 1	27° < ITA ≤ 55°	5	5	4	14	6 M / 8 F
Group 2	-1° < ITA ≤ 27°	6	5	6	17	9 M / 8 F
Group 3	ITA ≤ -1°	5	4	6	15	9 M / 6 F
Number of Subjects		16	14	16	46	24 M / 22 F
Number of Scans		64	56	64	184	

Scan #	Protocol 1	Protocol 2	Protocol 3
1	1064 nm, 100 mW/cm², 10 Hz	1064 nm, 150 mW/cm², 10 Hz	1064 nm, 150 mW/cm², 40 Hz
2	808 nm, 100 mW/cm², 10 Hz	808 nm, 150 mW/cm², 10 Hz	808 nm, 150 mW/cm², 40 Hz
3	1064 nm, 200 mW/cm², 10 Hz	1064 nm, 200 mW/cm², 40 Hz	1064 nm, 200 mW/cm², 40 Hz
4	808 nm, 200 mW/cm², 10 Hz	808 nm, 200 mW/cm², 40 Hz	808 nm, 200 mW/cm², 40 Hz
M / F	8 M / 8 F	7 M / 7 F	9 M / 7 F

Table 2. tPBM treatment parameters.

Parameter	Value
Duty cycle	50%
Beam spot size at stimulation site (cm^2)	≈ 1 cm^2
Wavelength (nm)	808 or 1064
Distance from scalp (cm)	~0
Pulsation frequency (Hz)	10 or 40
Irradiance at stimulation site (mW/cm^2)	100, 150, or 200
Duration of stimulation (minutes)	4
Radiant energy (J)	12.014, 18.021, or 24.028
Duty cycle	50%

2.3 EEG Acquisition

EEG was recorded at 1,000 Hz with a 256-channel Geodesic Net Amp 400 amplifier (Magstim Inc., Roseville, MN, USA) using saline electrodes (reference: Cz, <50 kΩ impedance, 0.024 µV amplitude resolution, 10-20 international placement system). A 20-minute break separated scans to avoid carryover effects. The data pipeline involved preprocessing, power and sample entropy analysis, and linear mixed-effect (LME) modeling (**Fig. 3**).

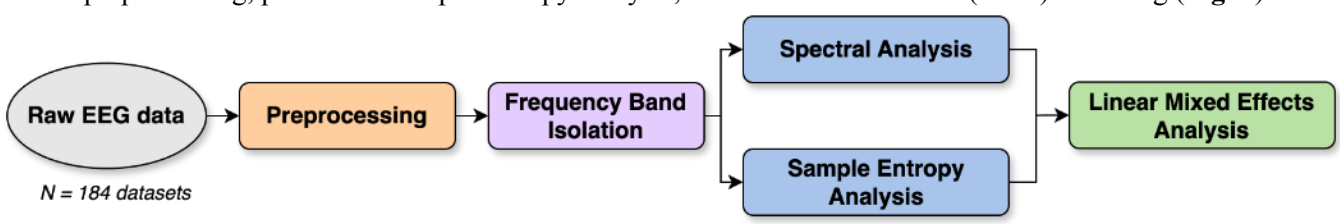

Figure 3. Summary of key stages in the data analysis pipeline.

2.4 Preprocessing

EEG data were processed using MATLAB (Mathworks Inc., Natick, MA, USA) with EEGLAB 2023.1. The preprocessing pipeline consisted of several sequential steps applied to each recording. Sixty-five face electrodes were removed from the 256-electrode array. Data were high-pass filtered at 1 Hz (to remove slow drifts while preserving delta activity) and downsampled to 125 Hz (providing adequate frequency resolution for low gamma analysis). Automated channel rejection was performed using the clean_rawdata algorithm with the following criteria: channels with <20% correlation to nearby channels were flagged as noisy (ChannelCriterion = 0.8), channels flat for >5 seconds were removed (FlatlineCriterion = 5), and line noise criterion was set to 4. This process excluded an average of 8.2 channels per dataset, yielding 182.8 channels across all preprocessed datasets. Independent Component Analysis (ICA) was performed using the extended infomax algorithm with automatic component ordering. Components were classified using ICLabel and those identified as eye movement artifacts, muscle activity, or line noise with probability >0.9 were automatically flagged and removed.

Each 12-minute recording was segmented into 60-second epochs for analysis using EEGLAB's eeg_regepochs function with non-overlapping windows without baseline removal or automatic epoch rejection. Additional data cleaning was applied to each epoch: channel-wise mean subtraction, outlier replacement using 5th-95th percentile thresholds with nearest-neighbor interpolation, mean restoration, and linear detrending to avoid drifts.

2.5 Band Extraction and EEG Metrics

Two complementary metrics were computed for each frequency band (delta: 1-3 Hz, theta: 4-8 Hz, alpha: 9-12 Hz, beta: 13-30 Hz, low gamma: 30-50 Hz) on a minute-by-minute scale:

- **Spectral Power**: Each 60-second epoch was windowed using a Hann function to minimize spectral leakage and Gibbs artifacts and subjected to FFT-based frequency-domain filtering with conjugate symmetry preservation. Spectral power was then calculated as the temporal variance of the band-limited signals after reconstruction using inverse FFT.
- **Sample Entropy (SampEn)**: Signal complexity was quantified using sample entropy with embedding dimension m=2 and tolerance r=0.2×SD, calculated on band-limited signals obtained via 4th-order Butterworth filtering. Additional information can be found in the supplementary materials.

Both metrics were normalized as percent change from the baseline period (minutes 1-4) using **Equation 2**:

$$Metric_{Norm}(\%) = \frac{Metric(t) - Metric_{Baseline}}{Metric_{Baseline}} \times 100 \qquad (2)$$

where $Metric(t)$ is power or SampEn at time t and $Metric_{Baseline}$ is the average across the baseline period.

2.6 Statistical Analysis

A general linear model (GLM) was applied to each electrode's $Metric(t)$ with a binary regressor (0: OFF, 1: ON) capturing tPBM responses in each scan. Electrodes with $p<0.05$ that were spatially adjacent (distance<0.05 normalized 2D units) and exhibited correlated time-courses (Pearson $r>0.5$) were grouped into candidate clusters which were then averaged and re-tested against a permutation-derived null distribution (500 shuffles). Clusters surpassing the null t-statistic distribution's 97.5th percentile were retained. Based on the sign of their original GLM t-statistics, electrodes within significant clusters were classified as displaying positive or negative modulation and assigned to anatomical regions (prefrontal, frontal, central, parietal, temporal, occipital) before hemispheric division.

Surviving electrodes were used in two analyses, whole-brain (global) and regional (based on anatomical region and hemisphere), where stepwise linear regression (MATLAB stepwiselm) identified relevant predictors of normalized EEG responses, R, grouped by frequency band, time period (during/post), and response direction (positive/negative). Candidate fixed effects included wavelength (808/1064 nm), frequency (10/40 Hz), irradiance (100/150/200 mW/cm^2), sex (male/female), and continuous ITAs (scaled by their range for better interpretability). Main effects and interactions were added iteratively from a constant-only model using default stepwiselm criteria ($p<0.05$ for entry/removal, FDR-corrected) and then used in LME models (MATLAB fitlme) with the general form shown in **Equation 3**:

$$R \sim Effect_1 + Effect_2 + Effect_1 : Effect_2 + (1 \mid Subject) \qquad (3)$$

where *Subject* was a random intercept representing inter-subject variability across repeated scans. To further assess potential inter-subject variability in parameter sensitivity, we additionally tested models with random slopes for core stimulation parameters (wavelength, frequency, irradiance) when present in the stepwise-selected predictors, shown in **Equation 4**:

$$R \sim SelectedEffects + (1 + SelectedEffects \mid Subject) \qquad (4)$$

Final significance was determined using FDR correction ($q<0.05$). More information on individual formulas can be found in **Supplementary Tables 6-13** of the supplementary materials.

3 RESULTS

3.1 tPBM's Online Effect on EEG Power

During tPBM, both wavelengths produced distinct scalp-wide frequency-specific modulations. Power changes exceeding 100% from baseline were considered outliers and excluded from visualizations. LH and RH denote left and right hemispheres, respectively.

808-nm stimulation demonstrated wavelength-specific spectral reorganization patterns that varied markedly with pulsation frequency. Delta power showed net reductions across both frequencies, with 40-Hz producing widespread decreases alongside localized increases in frontal, central, parietal, and left prefrontal regions (**Fig. 4-5**). While 10-Hz tPBM generated delta increases in occipital areas, the overall pattern shows delta-power decrease (**Fig. 4-5**). Theta power increased broadly except in prefrontal regions, with 40-Hz showing additional decreases in right central and parietal areas (**Fig. 4-5**).

The most striking 808-nm effects occurred in higher frequency bands, particularly alpha enhancement. Alpha power showed significantly greater global enhancement with 40 Hz compared to 10 Hz (q = 9.65e-09, unpaired t-test) (**Fig. 4**), with robust increases in posterior and bilateral regions (**Fig. 5b**) contrasting with more limited posterior increases at 10 Hz. Beta power remained stable at 10 Hz but increased modestly in frontal and central regions at 40-Hz (**Fig. 4b & 5b**). Notably, gamma power increases appeared the highest using 10 Hz stimulation, particularly in right parietal and temporal regions (**Fig. 4a & 5a**), with more modest effects at 40 Hz. This frequency-dependent pattern revealed that 808-nm tPBM at 40 Hz yielded the largest and most global alpha power increase among all tested conditions.

1064-nm tPBM produced fundamentally different spectral signatures characterized by enhanced low-frequency activity. Power changes with this wavelength were characterized by increased delta-band activity at both frequencies, contrasting sharply with the delta reductions observed with 808-nm (**Fig. 6**). While effects on theta, alpha, beta, and gamma bands appeared similar in magnitude to 808-nm, their spatial distribution was more widespread. Delta power exhibited larger RH frontal enhancement at 10 Hz (**Fig. 6a & 7a**) but smaller increases at 40 Hz (**Fig. 6b & 7b**). Theta power increased at 10 Hz (**Fig. 7a**) but remained largely unchanged at 40 Hz.

Higher-frequency responses with 1064 nm revealed optimal parameter combinations for specific frequency targeting. Alpha power showed distinct spatial patterns: 10 Hz produced global increases while 40 Hz generated focal occipital enhancement, both showing region- and hemisphere-dependent variations (**Fig. 7**). Most notably, 1064-nm tPBM at 40 Hz induced the greatest beta and gamma increases overall, with gamma showing robust, global enhancement that was significantly higher at 40 Hz than 10 Hz (q = 3.93e-18) (**Fig. 6-7**).

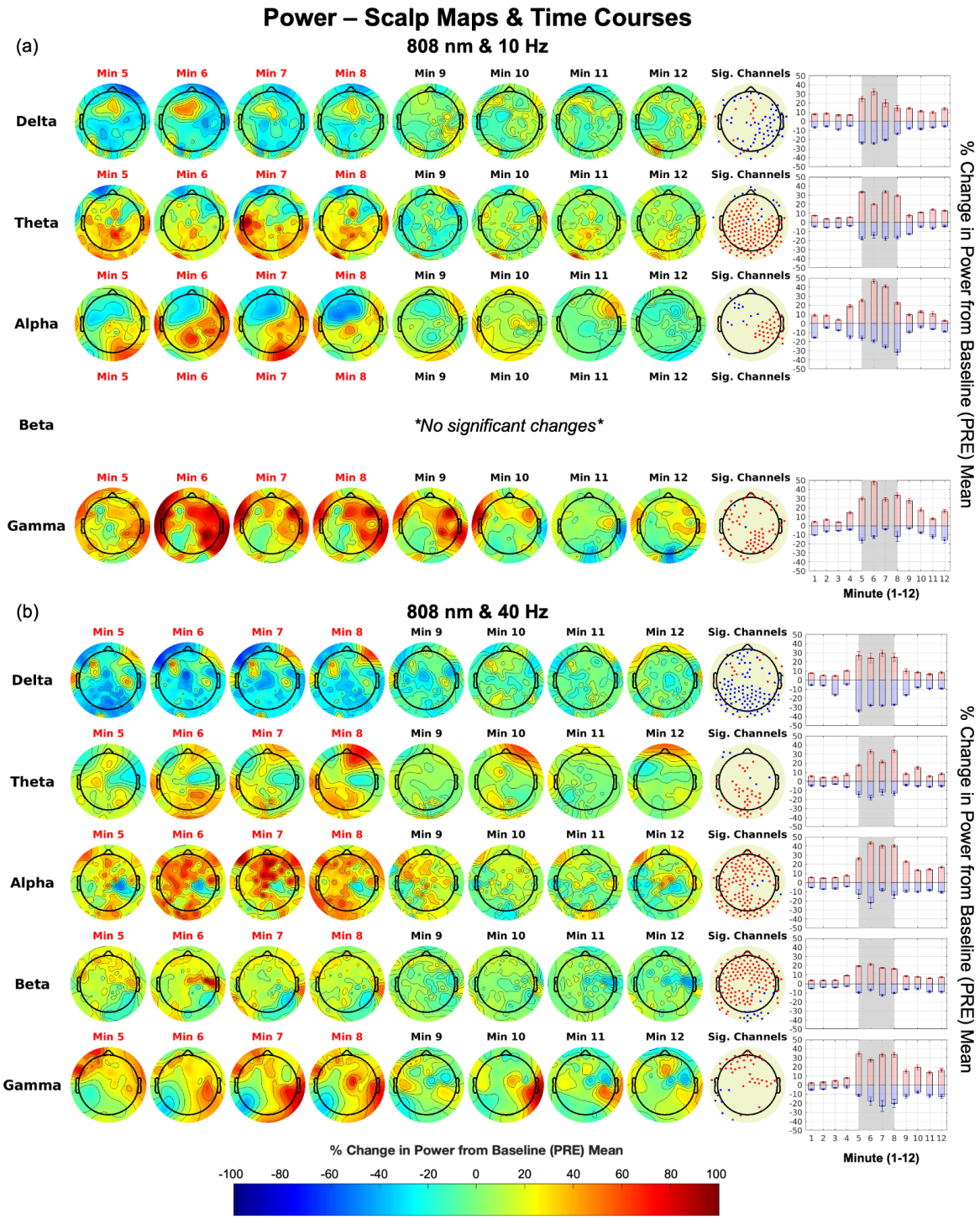

Figure 4. EEG power responses to 808-nm tPBM: minute-wise scalp topographies, channel markers representing significantly responding electrodes (positive shown in red; negative shown in blue), and corresponding time-course bar graphs for the 10 Hz (a) and 40 Hz (b) stimulation conditions. Topographic maps illustrate the percentage change in EEG power at each electrode relative to the pre-stimulus baseline (minutes 1-4). Electrodes showing significant responses (GLM analysis with stimulation period as predictor, $p<0.05$) are displayed in topographies, with red/blue markers in "Sig. Channels" column indicating positive/negative mean responses during stimulation (minutes 6-8). Bar graphs show group-mean percent change over time for significantly responding electrodes, with light red/blue bars representing averages of positive/negative responses respectively.

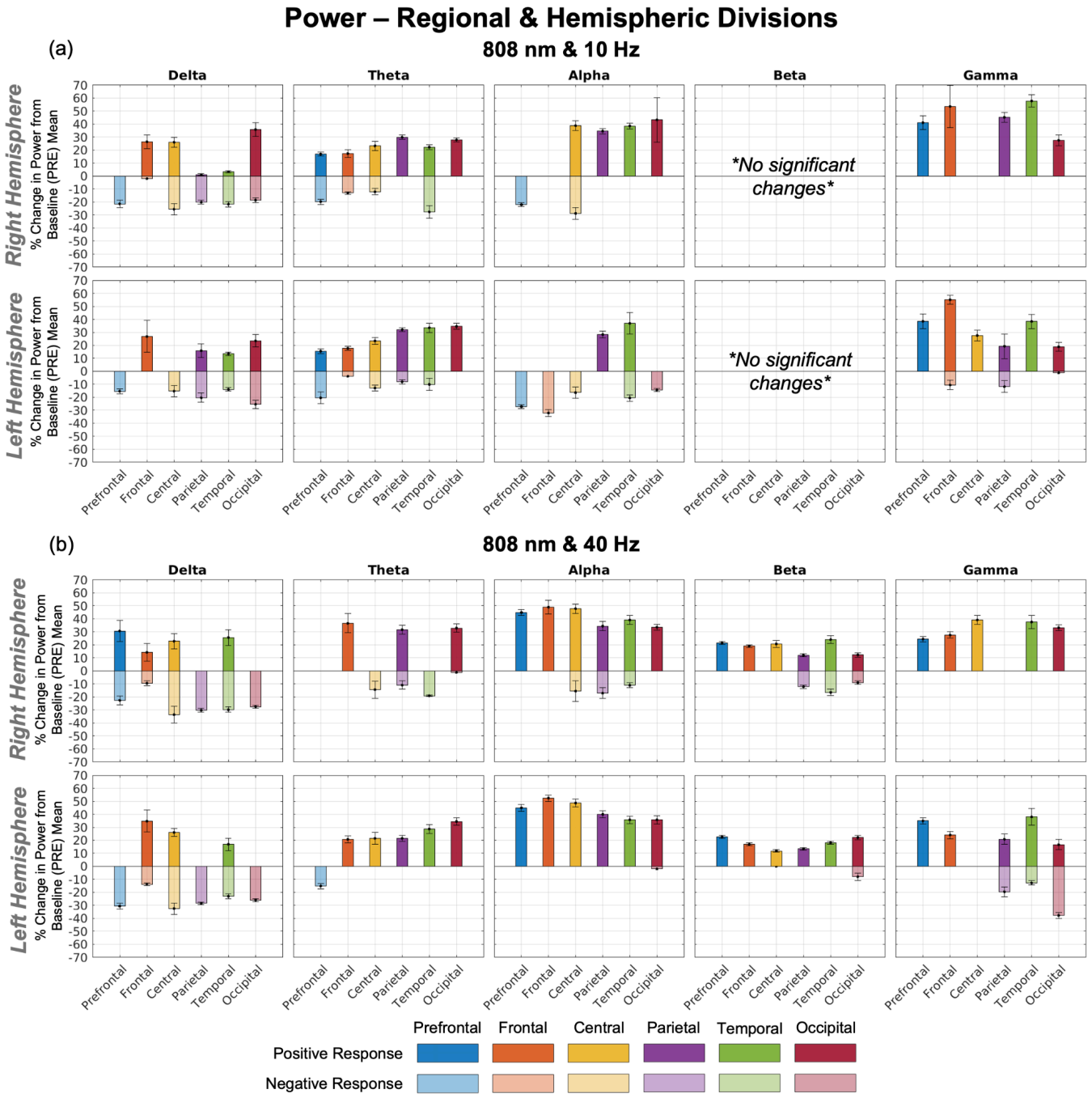

Figure 5. Hemispheric and regional EEG power responses during 808-nm tPBM: Average baseline-normalized band power during stimulation (minutes 6-8) for 10 Hz (a) and 40 Hz (b) conditions. Analysis restricted to electrodes showing significant responses to each specific wavelength-frequency combination (GLM; $p<0.05$). Data aggregated across datasets and grouped by brain region and hemisphere. Error bars show standard errors across significant electrodes within each region. Darker/lighter bars indicate positive/negative responses respectively.

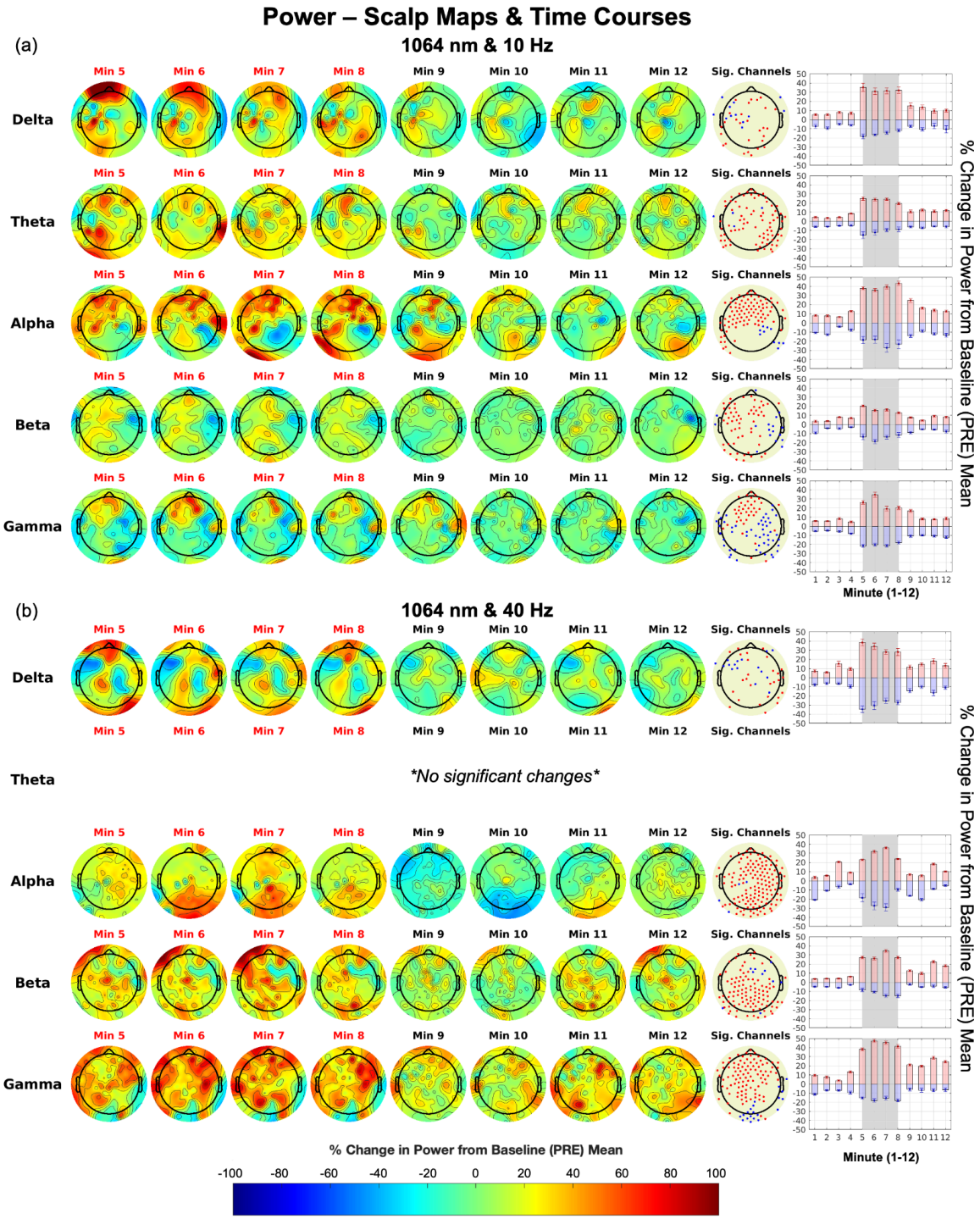

Figure 6. EEG power responses to 1064-nm tPBM: minute-wise scalp topographies, channel markers representing significantly responding electrodes (positive shown in red; negative shown in blue), and corresponding time-course bar graphs for the 10 Hz (a) and 40 Hz (b) stimulation conditions. Topographic maps illustrate the percentage change in EEG power at each electrode relative to the pre-stimulus baseline (minutes 1-4). Electrodes showing significant responses (GLM analysis with stimulation period as predictor, $p<0.05$) are displayed in topographies, with red/blue markers in "Sig. Channels" column indicating positive/negative mean responses during stimulation (minutes 6-8). Bar graphs show group-mean percent change over time for significantly responding electrodes, with light red/blue bars representing averages of positive/negative responses respectively.

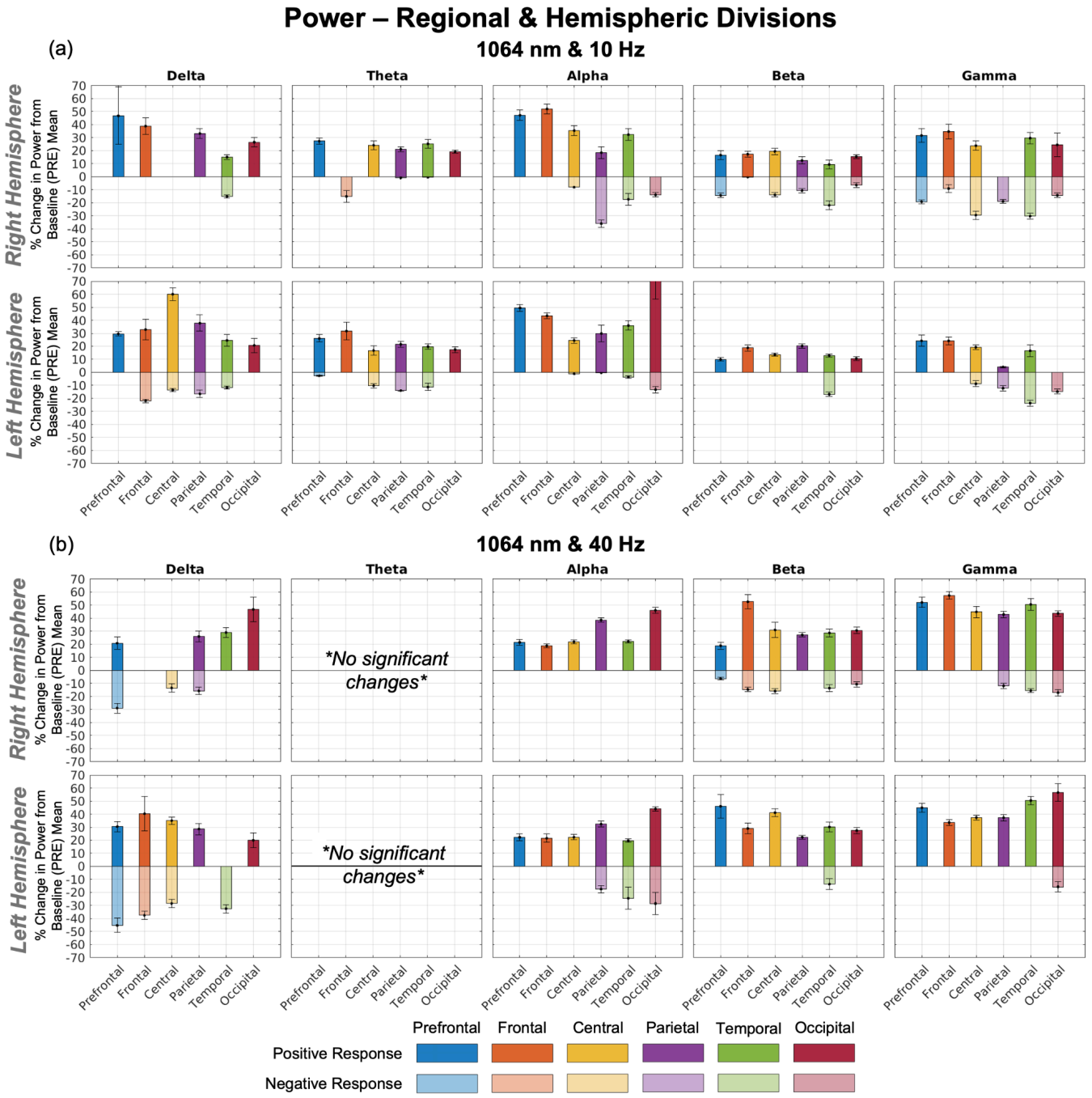

Figure 7. Hemispheric and regional EEG power responses during 1064-nm tPBM: Average baseline-normalized band power during stimulation (minutes 6-8) for 10 Hz (a) and 40 Hz (b) conditions. Analysis restricted to electrodes showing significant responses to each specific wavelength-frequency combination (GLM; $p<0.05$). Data aggregated across datasets and grouped by brain region and hemisphere. Error bars show standard errors across significant electrodes within each region. Darker/lighter bars indicate positive/negative responses respectively.

3.2 tPBM's Online Effect on EEG Sample Entropy

Sample entropy analysis revealed wavelength- and frequency-dependent changes in neural signal complexity and irregularity that were confined to the stimulation period. These complexity measures provide complementary insights into neural adaptability and network dynamics beyond traditional power analysis.

808-nm stimulation produced regionally specific entropy patterns that differed across frequency bands. Delta entropy increased in occipital areas and decreased in central regions (**Fig. 8-9**). Alpha entropy demonstrated consistent increases at both 10 Hz and 40 Hz, suggesting enhanced complexity in alpha-range oscillations regardless of the specific pulsation frequency. Beta entropy remained stable at 10 Hz but decreased across the scalp at 40 Hz, while gamma entropy remained consistently low at both frequencies.

1064-nm tPBM generated broader entropy enhancements concentrated in lower frequency bands. Delta and theta entropy increased extensively, with particularly pronounced effects at 10 Hz showing LH dominance (**Fig. 11a**). Alpha entropy exhibited region-specific patterns: increases occurred in occipital regions at 10 Hz and frontal regions at 40 Hz, while decreases emerged in other areas. Gamma entropy generally decreased during stimulation (**Fig. 11b**), contrasting with the robust gamma power increases observed with this wavelength.

3.3 tPBM's Offline Effect

The post-stimulation period (minutes 10-12) revealed differential persistence patterns across frequency bands and measures, providing insights into the temporal dynamics of tPBM effects.

Power changes showed frequency-band specific persistence patterns that varied by wavelength. Delta power returned to baseline across all conditions, while theta power remained mildly elevated following 808-nm stimulation but normalized more rapidly after 1064-nm protocols. Alpha power exhibited moderate persistence with 1064 nm at 10 Hz, contrasting with the rapid normalization observed after 808-nm stimulation (**Fig. 4 & 6**).

The most sustained effects occurred in higher-frequency bands, particularly with specific wavelength-frequency combinations. Beta and gamma power demonstrated the greatest persistence following 1064-nm stimulation at 40 Hz, primarily in frontal, central, and occipital regions (**Fig. 6**). Additionally, 808 nm produced sustained gamma power changes in right parietal and temporal regions at both frequencies (**Fig. 4**), suggesting wavelength-specific mechanisms of lasting neural modulation.

In contrast to power measures, entropy changes normalized rapidly across all frequency bands, indicating that complexity modulations were primarily stimulus-bound. This temporal dissociation between power and entropy responses suggests distinct underlying mechanisms, with power changes reflecting more sustained neural modulations while entropy effects represent network reorganization processes tied to the presence of the stimulus.

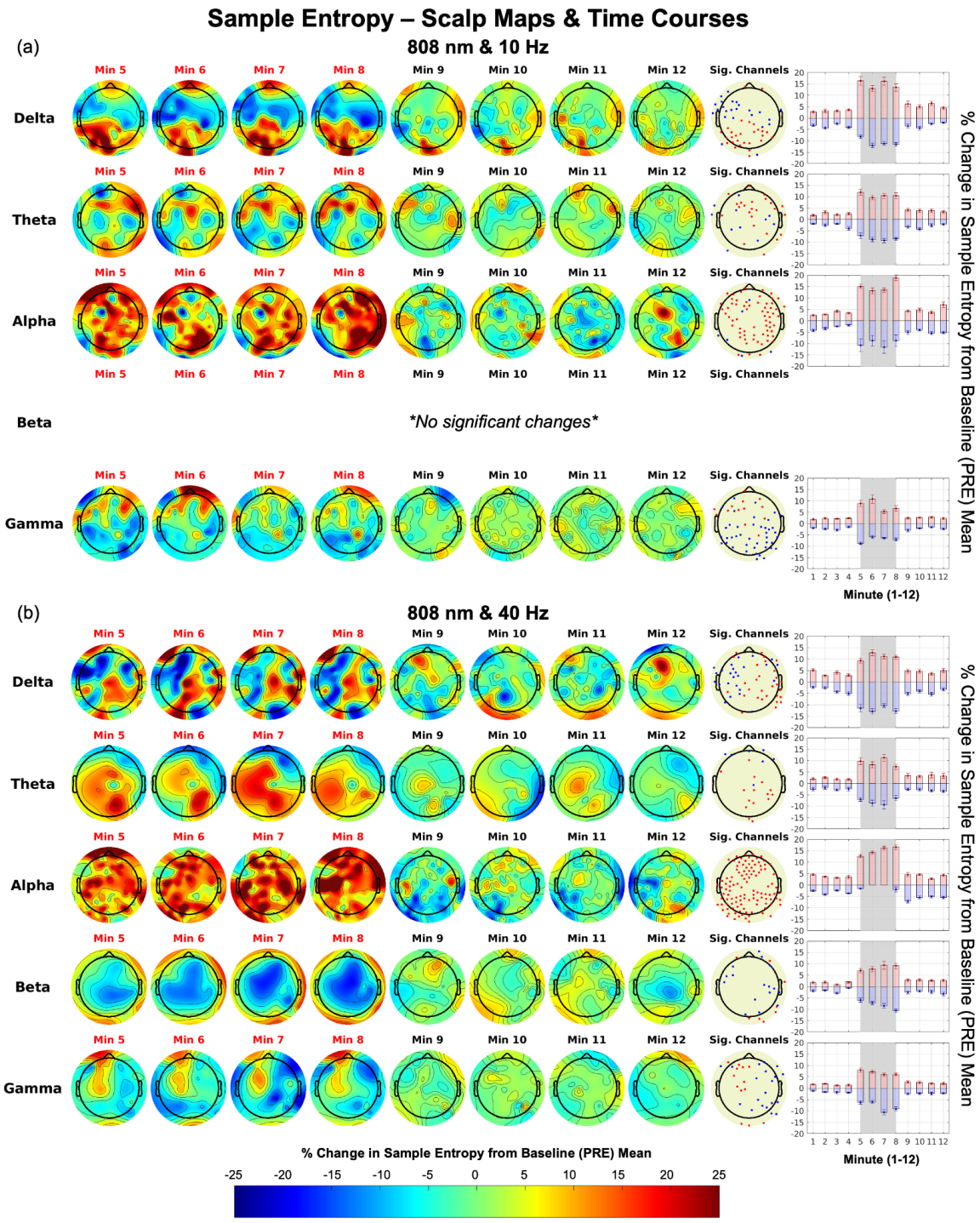

Figure 8. EEG sample entropy responses to 808-nm tPBM: minute-wise scalp topographies, channel markers representing significantly responding electrodes (positive shown in red; negative shown in blue), and corresponding time-course bar graphs for the 10 Hz (a) and 40 Hz (b) stimulation conditions. Topographic maps illustrate the percentage change in EEG SampEn at each electrode relative to the pre-stimulus baseline (minutes 1-4). Electrodes showing significant responses (GLM analysis with stimulation period as predictor, $p<0.05$) are displayed in topographies, with red/blue markers in "Sig. Channels" column indicating positive/negative mean responses during stimulation (minutes 6-8). Bar graphs show group-mean percent change over time for significantly responding electrodes, with light red/blue bars representing averages of positive/negative responses respectively.

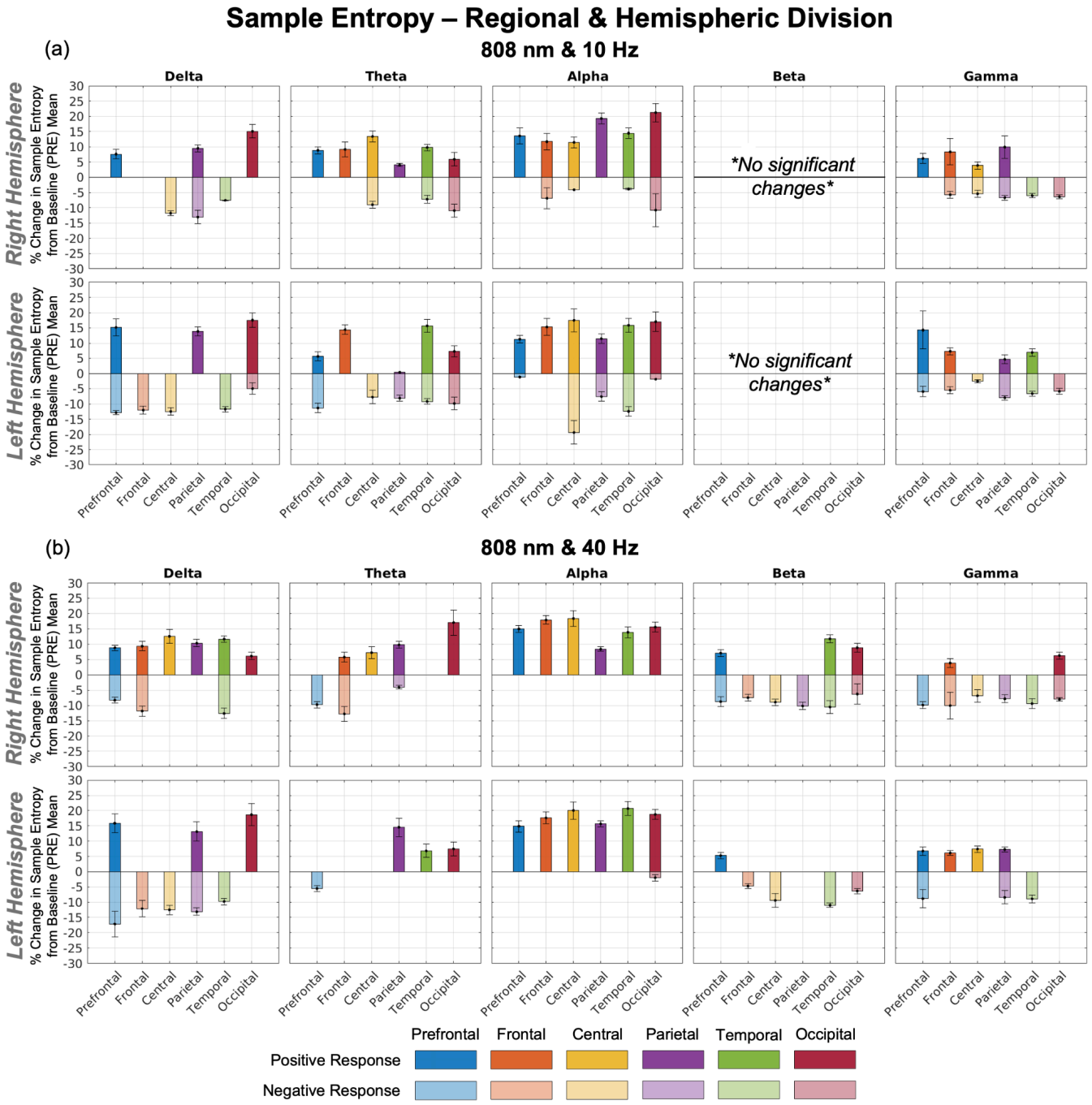

Figure 9. **Hemispheric and regional EEG sample entropy responses during 808-nm tPBM**: Average baseline-normalized band SampEn during stimulation (minutes 6-8) for 10 Hz (a) and 40 Hz (b) conditions. Analysis restricted to electrodes showing significant responses to each specific wavelength-frequency combination (GLM; $p<0.05$). Data aggregated across datasets and grouped by brain region and hemisphere. Error bars show standard errors across significant electrodes within each region. Darker/lighter bars indicate positive/negative responses respectively.

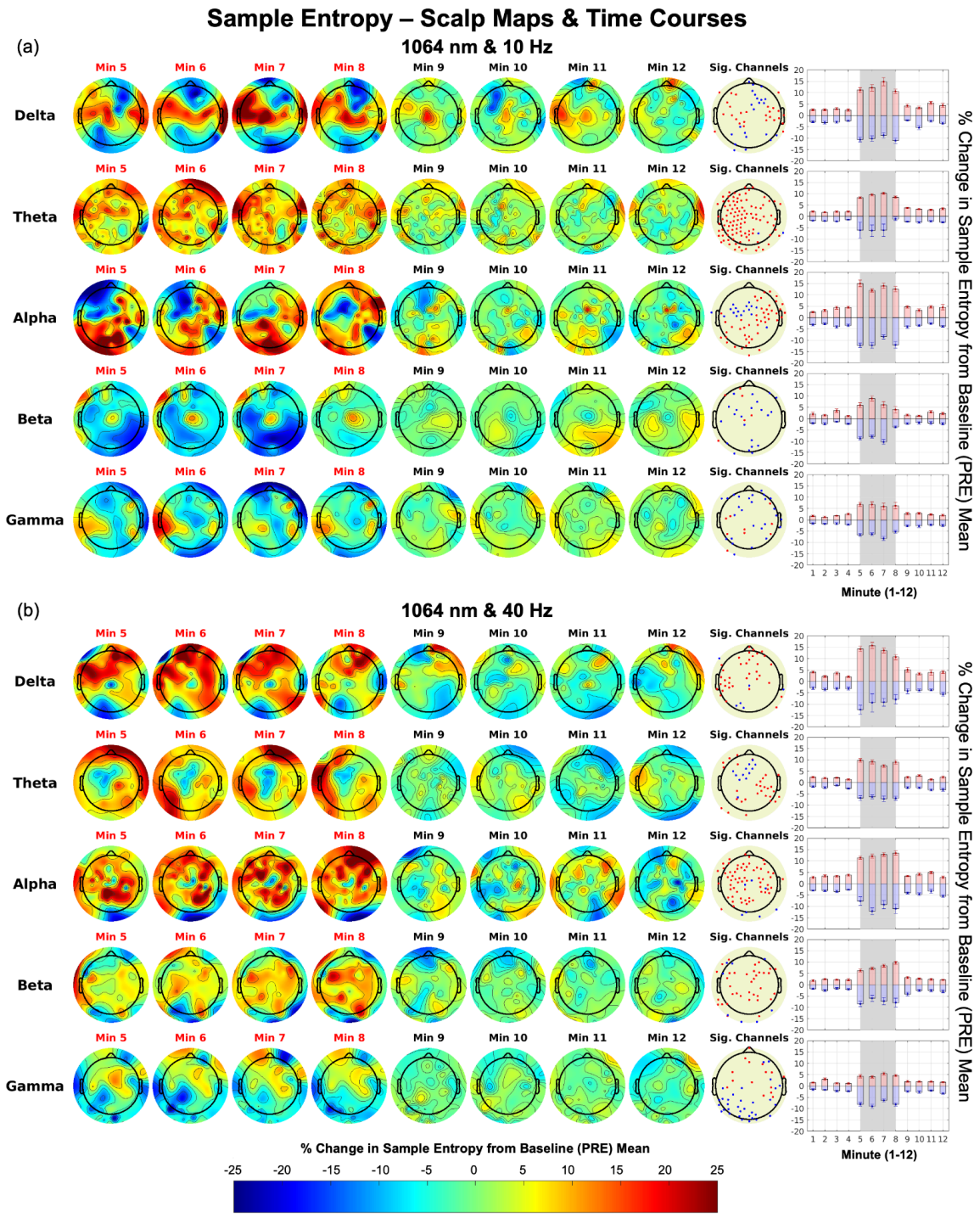

Figure 10. EEG sample entropy responses to 1064-nm tPBM: minute-wise scalp topographies, channel markers representing significantly responding electrodes (positive shown in red; negative shown in blue), and corresponding time-course bar graphs for the 10 Hz (a) and 40 Hz (b) stimulation conditions. Topographic maps illustrate the percentage change in EEG SampEn at each electrode relative to the pre-stimulus baseline (minutes 1-4). Electrodes showing significant responses (GLM analysis with stimulation period as predictor, $p<0.05$) are displayed in topographies, with red/blue markers in "Sig. Channels" column indicating positive/negative mean responses during stimulation (minutes 6-8). Bar graphs show group-mean percent change over time for significantly responding electrodes, with light red/blue bars representing averages of positive/negative responses respectively.

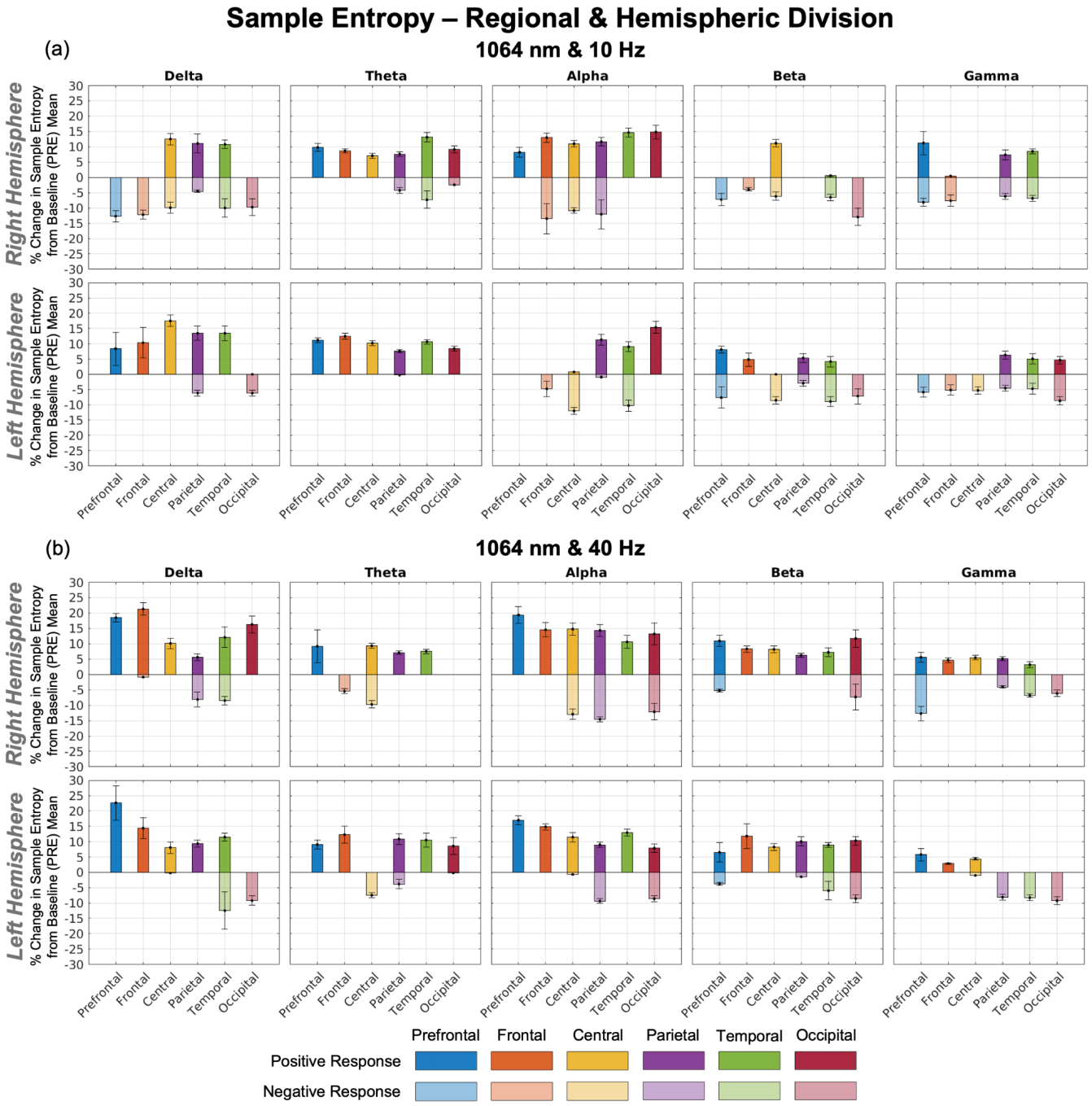

Figure 11. Hemispheric and regional EEG sample entropy responses during 1064-nm tPBM: Average baseline-normalized band SampEn during stimulation (minutes 6-8) for 10 Hz (a) and 40 Hz (b) conditions. Analysis restricted to electrodes showing significant responses to each specific wavelength-frequency combination (GLM; $p<0.05$). Data aggregated across datasets and grouped by brain region and hemisphere. Error bars show standard errors across significant electrodes within each region. Darker/lighter bars indicate positive/negative responses respectively.

3.4 Multi-Parameter Dependence of EEG Response During & Post-tPBM

LME analyses on baseline-normalized metrics during and post-tPBM were performed to distinguish online (minutes 6-8) and offline effects, including a whole-brain analysis investigating parameter and sex dependencies (**Supplementary Fig. 1**) and a region-separated analysis focusing on parameter effects alone (**Fig. 12**). Both modeling approaches (**Eq. 3 & 4**) yielded highly similar population-level estimates for effects that remained significant, confirming the robustness of our main findings and indicating minimal inter-subject variability in average parameter responses (**Supplementary Tables 6-13**). Only significant differences (FDR $q<0.05$ from both model results) among the tested parameter values are discussed below. ITA effects represent changes across the entire skin tone range (darkest to lightest). The terms "larger" and "smaller" are used to describe whether the specified response (positive or negative) was enhanced or reduced at that parameter value.

3.4.1 Online Effects

The significant dependencies associated with the online effect of tPBM on EEG power are illustrated in **Fig. 12a** and summarized in **Table 3 and Table 4**.

Table 3. Online effects of tPBM on EEG power, among positively responding significant electrodes.

EEG Power – Online Effects – Positive Responses						
		Delta	**Theta**	**Alpha**	**Beta**	**Gamma**
Wavelength		**Smaller** for 808 nm than 1064 nm, especially in the occipital region.			**Larger** for 808 nm than 1064 nm.	
Frequency		**Smaller** for 40 Hz than 10 Hz.	**Smaller** for 40 Hz than 10 Hz, especially in the temporal region.			**Larger** for 40 Hz than 10 Hz, especially in prefrontal, frontal, and central regions.
Irradiance				**Smaller** for 150 than 100 mW/cm^2.		
Skin tone	*Independent*		**Smaller** for lighter skin, especially in the frontal region.		**Larger** for lighter skin.	
	Frequency interaction					**Larger** for lighter skin, at 40 Hz.
Sex		**Larger** for males than females.				

Table 4. Online effects of tPBM on EEG power, among negatively responding significant electrodes.

EEG Power – Online Effects – Negative Responses						
		Delta	**Theta**	**Alpha**	**Beta**	**Gamma**
Wavelength		**Larger** for 808 nm than 1064 nm in the parietal region.				**Smaller** for 808 nm than 1064 nm, especially in the parietal and temporal region.
Frequency	*Independent*		**Larger** for 40 Hz than 10 Hz, especially in the occipital region.	**Larger** for 40 Hz than 10 Hz, especially in the occipital region.		
	Wavelength interaction					**Larger** for 40 Hz than 10 Hz, at 808 nm.
Skin tone		• **Smaller** for lighter skin in the parietal region. • **Larger** for lighter skin in the temporal region.	**Larger** for lighter skin.		**Smaller** for lighter skin, especial ly in the central region.	

The significant dependencies associated with the online effect of tPBM on EEG SampEn are illustrated in **Fig. 12b** and summarized in **Table 5 and Table 6**.

Table 5. Online effects of tPBM on EEG SampEn, among positively responding significant electrodes.

EEG SampEn – Online Effects – Positive Responses				
		Delta	**Theta**	**Beta**
Wavelength			**Smaller** for 808 nm than 1064 nm.	
Frequency	*Independent*	**Larger** for 40 Hz than 10 Hz in the prefrontal region.	**Smaller** for 40 Hz than 10 Hz, especially in the prefrontal and frontal region.	
	Wavelength interaction		**Larger** for 40 Hz than 10 Hz nm, for 808 nm.	
Irradiance				**Larger** for 200 than 100 mW/cm^2, especially in the prefrontal region.
Skin tone			**Larger** for lighter skin, especially in the frontal and central region.	
Sex				**Larger** for males than females.

Table 6. Online effects of tPBM on EEG SampEn, among negatively responding significant electrodes.

EEG SampEn – Online Effects – Negative Responses				
		Delta	**Theta**	**Alpha**
Irradiance				**Smaller** for 200 than 100 mW/cm., especially in the temporal region.
Skin tone		**Smaller** for lighter skin, especially in the temporal region.	**Smaller** for lighter skin, especially in the temporal region.	
Sex	*Independent*		**Larger** in males than females.	**Larger** in males than females.
	Irradiance interaction			Smaller in males than females, at both 150 mW/cm^2 and 200 mW/cm^2.

3.4.2 Offline Effects

The significant dependencies associated with the offline effect of tPBM on EEG power are illustrated in **Fig. 12c** and summarized in **Table 7 and Table 8**.

Table 7. Offline effects of tPBM on EEG power, among positively responding significant electrodes.

EEG Power – Offline Effects – Positive Responses					
		Delta	**Theta**	**Beta**	**Gamma**
Wavelength					**Smaller** for 808 nm than 1064 nm in the parietal region.
Frequency			**Smaller** for 40 Hz than 10 Hz, especially in the prefrontal region.		
Irradiance		• **Smaller** for 150 than 100 mW/cm^2 in the central region. • **Smaller** for 200 than 100 mW/cm^2.		**Smaller** for both 150 and 200 than 100 mW/cm^2.	
Skin tone	*Independent*			**Larger** in lighter skin, especially in the central region.	**Larger** in lighter skin in the frontal, central, and temporal region.
	Frequency interaction				**Larger** in lighter skin, at 40 Hz.
Sex	*Independent*		**Smaller** in males than females.		
	Frequency interaction		**Larger** in males than females, at 40 Hz.		

Table 8. Offline effects of tPBM on EEG power, among negatively responding significant electrodes.

EEG Power – Offline Effects – Negative Responses						
		Delta	**Theta**	**Alpha**	**Beta**	**Gamma**
Wavelength		**Smaller** for 808 nm than 1064 nm in the frontal region.				**Smaller** for 808 nm than 1064 nm, especially in the central region.
Frequency	*Independent*		**Smaller** for 40 Hz than 10 Hz in the temporal region.		**Smaller** for 40 Hz than 10 Hz in the temporal region.	
	Wavelength interaction					**Larger** for 40 Hz than 10 Hz, at 808 nm.
Irradiance		**Larger** for both 150 and 200 than 100 mW/cm^2.				
Skin tone				**Larger** in lighter skin in the frontal region.	**Larger** in lighter skin, especially in the occipital region.	
Sex	*Independent*	**Larger** in males than females.				
	Frequency interaction		**Smaller** in males than females, at 40 Hz.			
	Irradiance interaction	**Smaller** in males than females, at both 150 and 200 mW/cm^2.				

There were significant offline effects on SampEn but they were negligible.

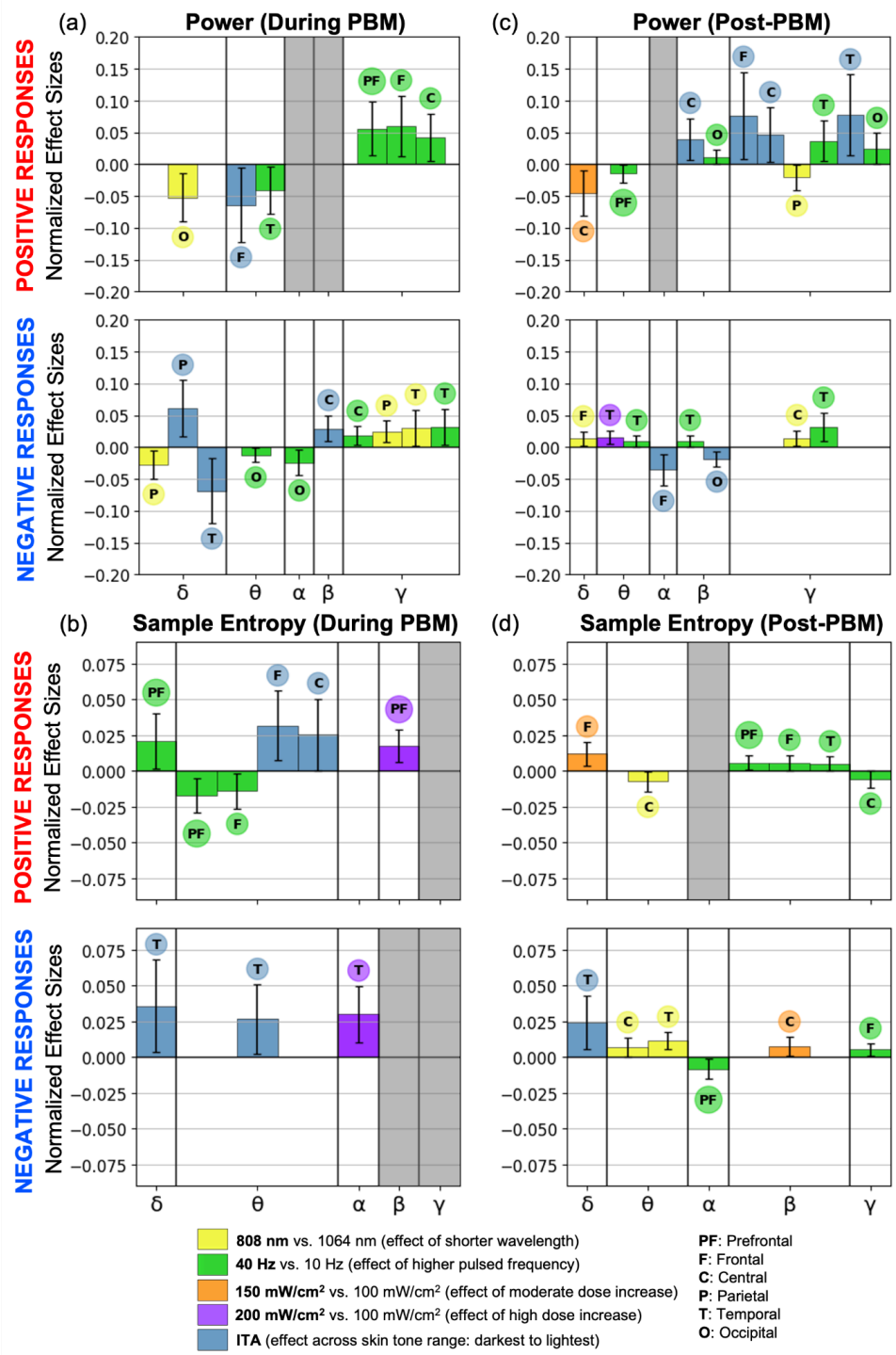

Figure 12. Regional tPBM parameter effects on EEG responses separated by frequency band and response direction: LME-derived significant effects showing the influence of parameters on EEG power (a, c) and SampEn (b, d) during and post-tPBM using normalized effect sizes (ES) which describe the influence each parameter has as a fraction of the EEG response (i.e. %Δpower or %Δentropy) at the reference values. Positive responses: positive ES = larger positive responses, negative ES = smaller positive responses. Negative responses: positive ES = smaller negative responses, negative ES = larger negative responses; all relative to reference values: 1064 nm wavelength, 10 Hz pulsation frequency, 100 mW/cm^2 irradiance. ITA ES represent the effect of lighter skin. Error bars: 95% confidence interval.

4 DISCUSSION

In this study, we quantified EEG responses to tPBM using two complementary metrics, band-limited spectral power and sample entropy (SampEn), to examine how tPBM parameters, skin tone, and sex shape neural dynamics. While EEG band power reflects the strength of neural oscillations linked to specific cognitive and physiological functions, SampEn captures the regularity or predictability of the time series within those bands. Together, these measures allowed us to identify not only how dominant specific rhythms were, but also how flexibly they were organized in time, revealing stimulus effects that would have been missed by power analysis alone. Across conditions, tPBM modulated both metrics in frequency- and region-specific ways, with power changes often persisting post-stimulation and SampEn effects largely stimulus-bound. Interpreting these findings requires understanding how EEG power and signal complexity vary across brain states, age, and health status. The following subsections discuss the parameter-dependent EEG responses we uncovered in each frequency band alongside the normative patterns and their implications for interpreting tPBM-induced changes.

4.1 The Effect of tPBM Parameters

4.1.1 Wavelength: 808 nm vs. 1064 nm

Both 808 nm and 1064 nm stimulation shifted spectral power from lower to higher frequencies during stimulation, with increases in global alpha and gamma activity. Delta power was more consistently reduced with 808 nm, whereas alpha and gamma increases were generally larger with 1064 nm (**Fig. 4-7, Tables 3-4**). These patterns suggest that while both wavelengths engage cortical networks during stimulation, 808 nm produces a stronger low-frequency suppression, and 1064 nm has a greater capacity to enhance higher-frequency oscillations, possibly reflecting its deeper tissue penetration.

At the lower end of the frequency spectrum, delta rhythms are most prominent during slow-wave sleep, supporting memory consolidation and glymphatic clearance (Léger et al., 2018; Reddy & van der Werf, 2020), but they also occur in quiet wakefulness as part of localized rest of inhibitory control processes (Harmony, 2013; Sachdev et al., 2015). Theta activity is closely linked to memory encoding and retrieval, attentional engagement, and frontal-midline executive control (Herweg et al., 2016; Karakaş, 2020; Klimesch, 1999; Klimesch et al., 2001). In our study, 808-nm tPBM produced more consistent delta power reductions than 1064 nm, potentially implying greater cortical activation and reduced inhibitory states, while both wavelengths showed broadly similar theta changes. These low-frequency reductions align with a shift toward a more alert and engaged state during tPBM.

In the mid to high-frequency range, alpha oscillations are often associated with cortical idling or active inhibition, but can also be a measure of neural efficiency by supporting the suppression of irrelevant stimuli (Bonnefond et al., 2017; Iemi et al., 2022; Palva & Palva, 2011). Here, 1064-nm stimulation produced stronger alpha power increases than 808 nm, suggesting more pronounced thalamocortical coordination and possibly greater efficiency in managing attentional resources. Beta increases, linked to motor readiness and sustained attention, were observed for both wavelengths, though they were smaller in magnitude than the changes seen in alpha and gamma. Often associated with perceptual binding, attentional selection, and memory operations, (Jadi et al., 2016; Nyhus & Curran, 2010; Wynn et al., 2023), gamma power increased under both wavelength conditions but was more strongly enhanced by 1064 nm. This may reflect its deeper reach into cortical and subcortical structures, supporting the integration of complex sensory and cognitive processes as well as heightened attention while video-watching. Another interesting observation at 1064 nm was a noticeable rebound in alpha and gamma power modulation around Minute 10/11 (**Fig. 6**) that aligns with the activation we see in R3 in the Wang et al. (2019) finding. It is worth noting that, despite their stimulation duration being longer (11 minutes), this relapse in activity appears around the same amount of time after the stimulation was turned off (two to three minutes) in both our results as well as theirs.

In terms of complexity changes measured by SampEn, the two wavelengths differed more clearly. For 808 nm, increases in SampEn were concentrated in the delta to alpha bands, with the largest change in alpha, while beta and gamma SampEn decreased, indicating a shift toward more synchronized fast oscillations. In contrast, 1064 nm increased SampEn across all frequency bands, including gamma, reflecting a broader enhancement of neural signal complexity and long-range network flexibility (Deligianni et al., 2014). Functionally, higher delta and theta SampEn

during wakefulness may support greater attentional readiness (Bruce et al., 2009), while increased alpha and gamma entropy may indicate improved information-carrying capacity and cognitive adaptability. Age-related declines in slow-band entropy (Pappalettera et al. 2023) mean that tPBM-induced increases here could represent a reversal toward healthier dynamics, possibly through improved astrocyte-mediated glymphatic function (Beard et al., 2021) or better subcortical-cortical coordination.

These wavelength differences may stem from distinct photobiological mechanisms at 808 nm and 1064 nm. The 808-nm wavelength, with higher photon energy (1.53 eV), is strongly absorbed by CCO (Van Lankveld et al., 2024b), the primary mitochondrial photoreceptor, triggering ATP production, nitric oxide (NO) release, calcium influx, and reactive oxygen species (ROS)-mediated signaling (Hamblin, 2018b; Y. Wang et al., 2017). These processes activate transcription factors and promote mitochondrial respiration and differentiation (de Freitas & Hamblin, 2016; Komarova et al., 2000; Zamani et al., 2020). This supports efficient superficial cortical modulation, despite higher susceptibility to melanin absorption and scattering. In contrast, 1064 nm penetrates deeper with less melanin absorption and scattering, reaching subcortical structures with minimal heating (Penberthy & Vorwaller, 2021). However, with lower photon energy (1.17 eV) and weaker CCO interaction, 1064 nm may rely more on alternative targets, such as light- and heat-gated ion channels (Hamblin, 2018b), potentially requiring higher irradiances or longer exposures for equivalent cellular effects. These physical and biological distinctions likely underpin the broader entropy increases and stronger alpha/gamma enhancements observed with 1064 nm, as well as the more selective low-frequency modulation seen with 808 nm. However, it is unclear how these mechanistic differences translate into a shift in brain rhythms to higher frequencies for 808nm and a shift to lower frequencies for 1064 nm.

4.1.2 Pulsation Frequency: 10 Hz vs. 40 Hz

While continuous tPBM has been widely studied, pulsed protocols can be advantageous due to reduced thermal buildup, possible recovery between pulses, and potential resonance effects with endogenous rhythms through frequency matching (Gillespie et al., 2017; Hashmi et al., 2010). The selected pulsation frequency may also drive resonance or entrainment effects (Kim et al., 2017; Tang, Qin, et al., 2023).

Across both wavelengths, 40 Hz consistently produced stronger modulation of spectral power across frequency bands, most prominently in alpha. When paired with 1064 nm, this frequency elicited particularly strong alpha and beta power increases. Beta modulation was especially sensitive to pulsation frequency, with the largest increase observed in the 1064 nm and 40 Hz condition. Given beta's association with executive control (Swann et al., 2009), working memory (Lundqvist et al., 2016; Miller et al., 2018), and sustained attention (Palacios-García et al., 2021; Cassim et al., 2001; Del Campo-Vera et al., 2021; Kilavik et al., 2013; Niemelä et al., 2025), these increases may partly reflect the experimental context: participants remained seated and still for extended periods, and protocols using 1064 nm and 40 Hz occurred later in the session sequence, possibly amplifying motor readiness and attentional engagement.

The 40 Hz frequency enhanced alpha and gamma power while suppressing delta and theta activity, particularly in lighter-skinned participants. Contrary to expectations that 10 Hz would strongly drive alpha rhythms through frequency matching, the 40 Hz condition yielded larger alpha increases, suggesting mechanisms beyond simple entrainment, potentially involving deeper or more widespread network engagement. For 808 nm, pulsing at 40 Hz produced robust posterior alpha and gamma gains alongside delta suppression, indicating a synergistic effect of high photon energy and frequency-specific modulation (**Fig. 4-5**).

Regarding complexity, 40 Hz increased alpha SampEn, reflecting inhibitory rhythms that were both strengthened and temporally flexible, while reducing gamma SampEn, consistent with transient synchronization of fast oscillations. By contrast, 10 Hz tended to increase SampEn in slower bands (delta/theta) despite modest power changes, implying enhanced flexibility in large-scale low-frequency networks without equivalent amplitude gains. Notably, the SampEn effects of 40 Hz were less dependent on wavelength than those of 10 Hz, which varied more strongly between 808 nm and 1064 nm.

Post-stimulation effects also revealed distinct temporal dynamics. 10 Hz better sustained inhibitory power effects in delta/theta power, while 40 Hz better maintained some high-frequency changes in interaction with biological factors (e.g., skin tone, sex). Complexity effects, however, were largely stimulus-bound, with minimal persistence for

either stimulated frequency. This separation between sustained amplitude shifts and transient complexity modulation highlights the importance of temporal resolution in protocol design.

4.1.3 Wavelength-Frequency Interactions

We observed strong wavelength-frequency interaction effects. With 808 nm stimulation at 10 Hz, negative power responses were most prominent from delta through alpha. However, when the pulsation rate was increased to 40 Hz, these reductions in delta and theta power became even more pronounced with 808 nm than with 1064 nm. This pattern aligns with 808 nm's stronger CCO absorption and greater sensitivity to pulsed delivery, suggesting that millisecond-scale timing effects on mitochondrial respiration and calcium signaling may contribute to these frequency-specific responses (Bertero & Maack, 2018; Patergnani et al., 2011; Stoler et al., 2022).

Entropy analyses aligned with this specificity. For 808 nm pulsed at 40 Hz, delta and theta entropy increased (**Supplementary Fig. 1**), indicating greater temporal variability in slow-band activity relative to baseline. Interestingly, at 10 Hz, 808 nm unexpectedly produced the largest gamma power increases (**Table 4**). This points to additional wavelength-specific mechanisms, potentially mitochondrial or ion-channel mediated, that operate beyond simple frequency matching.

Overall, 808 nm tended to elicit concurrent increases in high-frequency power and SampEn, consistent with oscillations that were both stronger and more adaptable. In contrast, 1064 nm more often combined increases in low-frequency power with higher SampEn (reflecting reduced slow-wave regularity) and increases in high-frequency power with lower SampEn (indicating greater synchronization). Taken together, these patterns suggest that 808 nm at 40 Hz preferentially promotes both strength and flexibility in high-frequency rhythms, while 1064 nm produces broader, deeper, but less frequency band-selective changes across the spectrum.

4.2 The Effect of Biological Factors

4.2.1 Skin Tone Dependence

Individual differences in epidermal melanin, as a prominent chromophore, directly affects light penetration, scattering, and absorption within neural tissues (Cassano et al., 2019; Li et al., 2017; Palamoni et al., 2022; Van Lankveld et al., 2024a). In our study, skin tone was a moderate predictor of online power changes, primarily in low frequencies: lighter-skinned participants showed mixed delta responses and reduced positive theta power. Post-stimulation, skin tone effects became stronger, with lighter skin linked to larger positive beta/gamma and smaller negative alpha/beta responses (4-8% ES) (**Fig. 12**), suggesting that higher-frequency modulation persists longer after tPBM in this group.

Unlike power, skin tone-dependent entropy responses were smaller and largely restricted to low frequencies during stimulation. Lighter-skinned participants showed greater positive theta entropy responses and smaller negative delta/theta entropy responses (~2.5% ES), indicating that melanin influences amplitude more than complexity in these bands. Notably, skin tone also interacted with frequency: lighter skin amplified gamma power gains at 40-Hz pulsation frequency during and post-tPBM, suggesting enhanced resonance or network recruitment in this subgroup.

We also uncovered frequency-skin tone interactions in gamma power responses with 40-Hz pulsation frequency: lighter skin amplified the positive effects of 40-Hz tPBM both during (normalized ES 10%) and, to a lesser extent, post-stimulation (5% ES), indicating a potential skin-tone mediated frequency-matching effect (**Supplementary Fig. 1**). This frequency-specific interaction shows that 40-Hz protocols may offer particular advantages for individuals with lighter skin tones. Although melanin effects were not significantly more limiting for 808 nm than 1064 nm, the consistent enhancement in lighter skin tones underscores the need for personalized dosimetry approaches. Future work could explore alternate delivery routes such as intranasal application for reduced melanin interference (Cichorek et al., 2013).

4.2.2 Sex Dependence and Interactions with Dose Parameters

Sex differences in EEG physiology are well-documented, with females typically showing higher resting power in alpha to gamma bands (Cave & Barry, 2021; Jausovec & Jausovec, 2010). Previous PBM studies have not identified statistically significant sex-dependence cognitive outcomes (Qi et al., 2021). However, our results show subtle sex-specific EEG effects. During stimulation, females had smaller positive delta power (4% ES) and smaller negative alpha entropy responses (3% ES) than males; post-stimulation, they showed larger negative theta power responses (3% ES) (**Supplementary Fig. 1**). Furthermore, we also saw interesting irradiance-sex interactions, particularly at 200 mW/cm2, with females showing larger negative alpha entropy responses during stimulation compared to males.

These differences may reflect estrogen's role in modulating mitochondrial sensitivity to tPBM (Rettberg et al., 2014). Estrogen receptor-mediated transcriptional regulation (Brinton, 2008; Chen et al., 2004; Irwin et al., 2012; Stirone et al., 2005; Yang et al., 2004) supports glucose transport, aerobic glycolysis, and mitochondrial bioenergetics (Mannella & Brinton, 2006; Nilsen et al., 2006; Nilsen & Brinton, 2004; Nilsen & Diaz Brinton, 2003). This may enhance tPBM responsiveness in females, particularly for protocols strongly engaging CCO (e.g., 808 nm), while males show more uniform but less dose-sensitive complexity changes.

4.3 Limitations and Future Work

While our work revealed significant dependences of the band-specific EEG responses on wavelength, frequency, and irradiance, several limitations constrain the generalizability and clinical translation of our findings. First, this study is limited to examining the effect of dose parameters, skin tone and sex. Given our findings of pronounced skin tone and sex dependencies, future studies could examine how changes in melanin distribution, hormonal fluctuations, and cortical thickness due to factors such as age interact with the parameter effects we identified. tPBM was also applied exclusively to the rPFC, restricting insights into parameter effects at other critical sites such as DMN nodes or the motor cortex due to their relevance in neurodegenerative diseases. The regional specificity we observed further suggests that optimal parameters may be site-dependent. Future work can compare parameter responses across multiple brain regions to determine whether our prefrontal findings generalize or require region-specific optimization.

Additionally, our irradiance range, while physiologically relevant, may not capture the full therapeutic window. Testing was limited to 100-200 mW/cm^2 to avoid thermal sensations, potentially missing higher intensities that could reveal biphasic dose-response patterns predicted by PBM theory (Huang et al., 2011). The significant irradiance-sex interactions also suggest that optimal power densities may require sex-specific modification, but our constrained range prevents specific dose-response characterization. The temporal resolution of our analysis, while revealing distinct online versus offline patterns, cannot capture the full time-course of tPBM effects. Our short during and post-tPBM analysis windows may miss later onset effects or longer-lasting changes that could inform optimal treatment scheduling. The rapid normalization of entropy changes that contrasted with sustained power effects further suggests complex temporal dynamics that warrant investigation across multiple timescales, from seconds to potentially even hours post-treatment. Variations in the distance between the laser and the cortex were also not accounted for as this required precisely measuring each tissue layer's optical properties of light scattering and absorption which were not feasible due to insufficient data.

Integrating EEG with hemodynamic imaging (e.g., fMRI) would also help clarify how tPBM influences metabolic and vascular systems. Such multimodal approaches could enable simultaneous measurement of cerebral blood flow, cerebral metabolic rate of oxygen consumption ($CMRO_2$), and neural oscillatory activity, providing crucial insights into whether the observed EEG changes reflect direct mitochondrial stimulation, improved cerebrovascular function, or both. Finally, exploring delivery routes that minimize melanin interference, like intranasal application, could broaden accessibility and efficacy, a treatment approach we plan to investigate in the future.

5 CONCLUSIONS

This study is the first to demonstrate how tPBM stimulation parameters interact with biological factors to shape neural oscillatory power and signal complexity in real-time. Our findings reveal that the neural response to

tPBM depends on interactions between wavelength, frequency, irradiance, skin tone, and sex, challenging current practices of parameter adoptions and stressing the need for personalized protocols. Multiple lines of evidence support 808-nm tPBM at 40 Hz as being more effective in shifting the EEG power hierarchy from low- to high-frequency, considered important for improving cognition. Concurrently, 1064-nm stimulation at 10 Hz showed advantages for sustained lower-frequency modulation. Moreover, we show that distinct mechanisms of neural activity, such as neural oscillation power and entropy, can be strategically targeted depending on whether immediate network reorganization or lasting oscillatory enhancement is desired. Furthermore, the consistent enhancement of responses in lighter skin tones and the sex-dependent frequency interactions demonstrate that demographic factors are not merely confounding variables but critical determinants of treatment efficacy. These findings necessitate the development of individualized dosing protocols that account for optical and physiological differences to ensure equitable therapeutic outcomes across diverse populations. By establishing EEG as a sensitive, real-time biomarker of tPBM effects, our multidimensional parameter results provide a roadmap for advancing tPBM from a one-size-fits-all approach toward more precise protocols.

6 ACKNOWLEDGMENTS

This work was supported by funding from the Ontario Centre for Innovation, the Natural Sciences and Engineering Research Council of Canada, Ydessa Hendeles Graduate Scholarship, and Vielight Inc.

7 REFERENCES

Adler, G., Brassen, S., Chwalek, K., Dieter, B., & Teufel, M. (2004). Prediction of treatment response to rivastigmine in Alzheimer's dementia. *Journal of Neurology, Neurosurgery, and Psychiatry*, *75*(2), 292–294. https://www.ncbi.nlm.nih.gov/pubmed/14742608

Babiloni, C., Blinowska, K., Bonanni, L., Cichocki, A., De Haan, W., Del Percio, C., Dubois, B., Escudero, J., Fernández, A., Frisoni, G., Guntekin, B., Hajos, M., Hampel, H., Ifeachor, E., Kilborn, K., Kumar, S., Johnsen, K., Johannsson, M., Jeong, J., … Randall, F. (2020). What electrophysiology tells us about Alzheimer's disease: a window into the synchronization and connectivity of brain neurons. *Neurobiology of Aging*, *85*, 58–73. https://doi.org/10.1016/j.neurobiolaging.2019.09.008

Barry, R. J., & De Blasio, F. M. (2017). EEG differences between eyes-closed and eyes-open resting remain in healthy ageing. *Biological Psychology*, *129*, 293–304. https://doi.org/10.1016/j.biopsycho.2017.09.010

Beard, E., Lengacher, S., Dias, S., Magistretti, P. J., & Finsterwald, C. (2021). Astrocytes as key regulators of brain energy metabolism: New therapeutic perspectives. *Frontiers in Physiology*, *12*, 825816. https://doi.org/10.3389/fphys.2021.825816

Berger, H. (1929). Über das Elektrenkephalogramm des Menschen. *Archiv für Psychiatrie und Nervenkrankheiten*, *87*(1), 527–570. https://doi.org/10.1007/bf01797193

Bertero, E., & Maack, C. (2018). Calcium signaling and reactive oxygen species in mitochondria. *Circulation Research*, *122*(10), 1460–1478. https://doi.org/10.1161/CIRCRESAHA.118.310082

Bonnefond, M., Kastner, S., & Jensen, O. (2017). Communication between brain areas based on nested oscillations. *eNeuro*, *4*(2). https://doi.org/10.1523/ENEURO.0153-16.2017

Brinton, R. D. (2008). The healthy cell bias of estrogen action: mitochondrial bioenergetics and neurological implications. *Trends in Neurosciences*, *31*(10), 529–537. https://doi.org/10.1016/j.tins.2008.07.003

Bruce, E. N., Bruce, M. C., & Vennelaganti, S. (2009). Sample entropy tracks changes in electroencephalogram power spectrum with sleep state and aging. *Journal of Clinical Neurophysiology: Official Publication of the American Electroencephalographic Society*, *26*(4), 257–266. https://doi.org/10.1097/WNP.0b013e3181b2f1e3

Cassano, P., Tran, A. P., Katnani, H., Bleier, B. S., Hamblin, M. R., Yuan, Y., & Fang, Q. (2019). Selective photobiomodulation for emotion regulation: model-based dosimetry study. *Neurophotonics*, *6*(1), 015004. https://doi.org/10.1117/1.NPh.6.1.015004

Cassim, F., Monaca, C., Szurhaj, W., Bourriez, J. L., Defebvre, L., Derambure, P., & Guieu, J. D. (2001). Does post-movement beta synchronization reflect an idling motor cortex? *Neuroreport*, *12*(17), 3859–3863.

https://doi.org/10.1097/00001756-200112040-00051
Cave, A. E., & Barry, R. J. (2021). Sex differences in resting EEG in healthy young adults. *International Journal of Psychophysiology: Official Journal of the International Organization of Psychophysiology*, *161*, 35–43. https://doi.org/10.1016/j.ijpsycho.2021.01.008
Chan, A. S., Lee, T. L., Yeung, M. K., & Hamblin, M. R. (2019). Photobiomodulation improves the frontal cognitive function of older adults. *International Journal of Geriatric Psychiatry*, *34*(2), 369–377. https://doi.org/10.1002/gps.5039
Chen, J. Q., Eshete, M., Alworth, W. L., & Yager, J. D. (2004). Binding of MCF-7 cell mitochondrial proteins and recombinant human estrogen receptors alpha and beta to human mitochondrial DNA estrogen response elements. *Journal of Cellular Biochemistry*, *93*(2), 358–373. https://doi.org/10.1002/jcb.20178
Cichorek, M., Wachulska, M., Stasiewicz, A., & Tymińska, A. (2013). Skin melanocytes: biology and development. *Advances in Dermatology and Allergology/Postępy Dermatologii I Alergologii*, *30*(1), 30. https://doi.org/10.5114/pdia.2013.33376
de Freitas, L. F., & Hamblin, M. R. (2016). Proposed mechanisms of photobiomodulation or low-level light therapy. *IEEE Journal of Selected Topics in Quantum Electronics: A Publication of the IEEE Lasers and Electro-Optics Society*, *22*(3), 348–364. https://doi.org/10.1109/JSTQE.2016.2561201
Del Campo-Vera, R. M., Tang, A. M., Gogia, A. S., Chen, K.-H., Sebastian, R., Gilbert, Z. D., Nune, G., Liu, C. Y., Kellis, S., & Lee, B. (2021). Neuromodulation in beta-band power between movement execution and inhibition in the human hippocampus. *Neuromodulation: Journal of the International Neuromodulation Society*, *25*(2), 232–244. https://doi.org/10.1111/ner.13486
Gal, S., Coldham, Y., Tik, N., Bernstein-Eliav, M., & Tavor, I. (2022). Act natural: Functional connectivity from naturalistic stimuli fMRI outperforms resting-state in predicting brain activity. *NeuroImage*, *258*(119359), 119359. https://doi.org/10.1016/j.neuroimage.2022.119359
Getzmann, S., Gajewski, P. D., Schneider, D., & Wascher, E. (2024). Resting-state EEG data before and after cognitive activity across the adult lifespan and a 5-year follow-up. *Scientific Data*, *11*(1), 988. https://doi.org/10.1038/s41597-024-03797-w
Gillespie, J. B., Maclean, M., Given, M. J., Wilson, M. P., Judd, Timoshkin, I. V., & MacGregor, S. J. (2017). Efficacy of Pulsed 405-nm Light-Emitting Diodes for Antimicrobial Photodynamic Inactivation: Effects of Intensity, Frequency, and Duty Cycle. *Photomedicine and Laser Surgery*, *35*(3). https://doi.org/10.1089/pho.2016.4179
Gonzalez-Lima, F., & Barrett, D. W. (2014). Augmentation of cognitive brain functions with transcranial lasers. *Frontiers in Systems Neuroscience*, *8*. https://doi.org/10.3389/fnsys.2014.00036
Hamblin, M. R. (2018a). Mechanisms and mitochondrial redox signaling in photobiomodulation. *Photochemistry and Photobiology*, *94*(2), 199–212. https://doi.org/10.1111/php.12864
Hamblin, M. R. (2018b). Photobiomodulation for traumatic brain injury and stroke. *Journal of Neuroscience Research*, *96*(4), 731–743. https://doi.org/10.1002/jnr.24190
Harmony, T. (2013). The functional significance of delta oscillations in cognitive processing. *Frontiers in Integrative Neuroscience*, *7*, 83. https://doi.org/10.3389/fnint.2013.00083
Hashmi, J. T., Huang, Y.-Y., Sharma, S. K., Kurup, D. B., De Taboada, L., Carroll, J. D., & Hamblin, M. R. (2010). Effect of pulsing in low-level light therapy. *Lasers in Surgery and Medicine*, *42*(6), 450–466. https://doi.org/10.1002/lsm.20950
Henderson, T. A., & Morries, L. D. (2015). Near-infrared photonic energy penetration: can infrared phototherapy effectively reach the human brain? *Neuropsychiatric Disease and Treatment*, *11*, 2191–2208. https://doi.org/10.2147/NDT.S78182
Hennessy, M., & Hamblin, M. R. (2017). Photobiomodulation and the brain: a new paradigm. *Journal of Optics (2010)*, *19*(1), 013003. https://doi.org/10.1088/2040-8986/19/1/013003
Herweg, N. A., Apitz, T., Leicht, G., Mulert, C., Fuentemilla, L., & Bunzeck, N. (2016). Theta-alpha oscillations bind the hippocampus, prefrontal cortex, and striatum during recollection: Evidence from simultaneous EEG-fMRI. *The Journal of Neuroscience: The Official Journal of the Society for Neuroscience*, *36*(12), 3579–3587. https://doi.org/10.1523/JNEUROSCI.3629-15.2016
Hess, C., Levy, B., Hashmi, A. Z., Hogan, J., Greenspan, S., Elber, A., Falcon, K., & Driscoll, D. F. (2020). Subjective versus objective assessment of cognitive functioning in primary care. *Journal of the American Board of Family*

Medicine: JABFM, *33*(3), 417–425. https://doi.org/10.3122/jabfm.2020.03.190265
Huang, Y.-Y., Sharma, S. K., Carroll, J., & Hamblin, M. R. (2011). Biphasic dose response in low level light therapy - an update. *Dose-Response: A Publication of International Hormesis Society*, *9*(4), 602–618. https://doi.org/10.2203/dose-response.11-009.Hamblin
Iaccarino, H. F., Singer, A. C., Martorell, A. J., Rudenko, A., Gao, F., Gillingham, T. Z., Mathys, H., Seo, J., Kritskiy, O., Abdurrob, F., Adaikkan, C., Canter, R. G., Rueda, R., Brown, E. N., Boyden, E. S., & Tsai, L.-H. (2016). Gamma frequency entrainment attenuates amyloid load and modifies microglia. *Nature*, *540*(7632), 230–235. https://doi.org/10.1038/nature20587
Iemi, L., Gwilliams, L., Samaha, J., Auksztulewicz, R., Cycowicz, Y. M., King, J.-R., Nikulin, V. V., Thesen, T., Doyle, W., Devinsky, O., Schroeder, C. E., Melloni, L., & Haegens, S. (2022). Ongoing neural oscillations influence behavior and sensory representations by suppressing neuronal excitability. *NeuroImage*, *247*(118746), 118746. https://doi.org/10.1016/j.neuroimage.2021.118746
Irwin, R. W., Yao, J., To, J., Hamilton, R. T., Cadenas, E., & Brinton, R. D. (2012). Selective oestrogen receptor modulators differentially potentiate brain mitochondrial function. *Journal of Neuroendocrinology*, *24*(1), 236–248. https://doi.org/10.1111/j.1365-2826.2011.02251.x
Jabès, A., Klencklen, G., Ruggeri, P., Antonietti, J.-P., Banta Lavenex, P., & Lavenex, P. (2021). Age-related differences in resting-state EEG and allocentric spatial working memory performance. *Frontiers in Aging Neuroscience*, *13*, 704362. https://doi.org/10.3389/fnagi.2021.704362
Jadi, M. P., Behrens, M. M., & Sejnowski, T. J. (2016). Abnormal gamma oscillations in N-methyl-D-aspartate receptor hypofunction models of schizophrenia. *Biological Psychiatry*, *79*(9), 716–726. https://doi.org/10.1016/j.biopsych.2015.07.005
Jahan, A., Nazari, M. A., Mahmoudi, J., Salehpour, F., & Salimi, M. M. (2019). Transcranial near-infrared photobiomodulation could modulate brain electrophysiological features and attentional performance in healthy young adults. *Lasers in Medical Science*, *34*(6), 1193–1200. https://doi.org/10.1007/s10103-018-02710-3
Jausovec, N., & Jausovec, K. (2010). Resting brain activity: differences between genders. *Neuropsychologia*, *48*(13), 3918–3925. https://doi.org/10.1016/j.neuropsychologia.2010.09.020
Jelic, V., Johansson, S.-E., Almkvist, O., Shigeta, M., Julin, P., Nordberg, A., Winblad, B., & Wahlund, L.-O. (2000). Quantitative electroencephalography in mild cognitive impairment: longitudinal changes and possible prediction of Alzheimer's disease. *Neurobiology of Aging*, *21*(4), 533–540. https://doi.org/10.1016/s0197-4580(00)00153-6
Jeong, J. (2004). EEG dynamics in patients with Alzheimer's disease. *Clinical Neurophysiology: Official Journal of the International Federation of Clinical Neurophysiology*, *115*(7), 1490–1505. https://doi.org/10.1016/j.clinph.2004.01.001
Kang, J.-H., Bae, J.-H., & Jeon, Y.-J. (2024). Age-related characteristics of resting-state electroencephalographic signals and the corresponding analytic approaches: A review. *Bioengineering (Basel, Switzerland)*, *11*(5). https://doi.org/10.3390/bioengineering11050418
Karakaş, S. (2020). A review of theta oscillation and its functional correlates. *International Journal of Psychophysiology: Official Journal of the International Organization of Psychophysiology*, *157*, 82–99. https://doi.org/10.1016/j.ijpsycho.2020.04.008
Kilavik, B. E., Zaepffel, M., Brovelli, A., MacKay, W. A., & Riehle, A. (2013). The ups and downs of β oscillations in sensorimotor cortex. *Experimental Neurology*, *245*, 15–26. https://doi.org/10.1016/j.expneurol.2012.09.014
Kim, H. B., Baik, K. Y., Choung, P.-H., & Chung, J. H. (2017). Pulse frequency dependency of photobiomodulation on the bioenergetic functions of human dental pulp stem cells. *Scientific Reports*, *7*(1), 15927. https://doi.org/10.1038/s41598-017-15754-2
Klimesch, W. (1999). EEG alpha and theta oscillations reflect cognitive and memory performance: a review and analysis. *Brain Research. Brain Research Reviews*, *29*(2-3), 169–195. https://doi.org/10.1016/s0165-0173(98)00056-3
Klimesch, W., Doppelmayr, M., Stadler, W., Pöllhuber, D., Sauseng, P., & Röhm, D. (2001). Episodic retrieval is reflected by a process specific increase in human electroencephalographic theta activity. *Neuroscience Letters*, *302*(1), 49–52. https://doi.org/10.1016/s0304-3940(01)01656-1
Komarova, S. V., Ataullakhanov, F. I., & Globus, R. K. (2000). Bioenergetics and mitochondrial transmembrane potential during differentiation of cultured osteoblasts. *American Journal of Physiology. Cell Physiology*, *279*(4),

C1220–C1229. https://doi.org/10.1152/ajpcell.2000.279.4.C1220
Léger, D., Debellemaniere, E., Rabat, A., Bayon, V., Benchenane, K., & Chennaoui, M. (2018). Slow-wave sleep: From the cell to the clinic. *Sleep Medicine Reviews*, *41*, 113–132. https://doi.org/10.1016/j.smrv.2018.01.008
Li, T., Xue, C., Wang, P., Li, Y., & Wu, L. (2017). Photon penetration depth in human brain for light stimulation and treatment: A realistic Monte Carlo simulation study. *Journal of Innovative Optical Health Sciences*, *10*(05), 1743002. https://doi.org/10.1142/S1793545817430027
López-Loeza, E., Rangel-Argueta, A. R., López-Vázquez, M. Á., Cervantes, M., & Olvera-Cortés, M. E. (2016). Differences in EEG power in young and mature healthy adults during an incidental/spatial learning task are related to age and execution efficiency. *Age (Dordrecht, Netherlands)*, *38*(2), 37. https://doi.org/10.1007/s11357-016-9896-z
Lundqvist, M., Rose, J., Herman, P., Brincat, S. L., Buschman, T. J., & Miller, E. K. (2016). Gamma and beta bursts underlie working memory. *Neuron*, *90*(1), 152–164. https://doi.org/10.1016/j.neuron.2016.02.028
Mannella, P., & Brinton, R. D. (2006). Estrogen receptor protein interaction with phosphatidylinositol 3-kinase leads to activation of phosphorylated Akt and extracellular signal-regulated kinase 1/2 in the same population of cortical neurons: a unified mechanism of estrogen action. *The Journal of Neuroscience: The Official Journal of the Society for Neuroscience*, *26*(37), 9439–9447. https://doi.org/10.1523/JNEUROSCI.1443-06.2006
Miller, E. K., Lundqvist, M., & Bastos, A. M. (2018). Working memory 2.0. *Neuron*, *100*(2), 463–475. https://doi.org/10.1016/j.neuron.2018.09.023
Motsenyat, A., Zhong, X. Z., Van Lankveld, H., Chen, J. X., Mathew, A., & Chen, J. J. (2025). Modulating cerebrospinal fluid dynamics using pulsed photobiomodulation: feasibility, parameter and skin-colour dependence. In *bioRxiv*. https://doi.org/10.1101/2025.05.06.652458
Neuhaus, E., Lowry, S. J., Santhosh, M., Kresse, A., Edwards, L. A., Keller, J., Libsack, E. J., Kang, V. Y., Naples, A., Jack, A., Jeste, S., McPartland, J. C., Aylward, E., Bernier, R., Bookheimer, S., Dapretto, M., Van Horn, J. D., Pelphrey, K., Webb, S. J., & The ACE GENDAAR Network. (2021). Resting state EEG in youth with ASD: age, sex, and relation to phenotype. *Journal of Neurodevelopmental Disorders*, *13*(1), 33. https://doi.org/10.1186/s11689-021-09390-1
Niemelä, L., Lerche, L., Illman, M., Kirveskari, E., Liljeström, M., Pauls, K. A. M., & Renvall, H. (2025). Cortical beta modulation during active movement is highly reproducible in healthy adults. *Journal of Neurophysiology*, *133*(4), 1067–1073. https://doi.org/10.1152/jn.00377.2024
Nilsen, J., & Brinton, R. D. (2004). Mitochondria as therapeutic targets of estrogen action in the central nervous system. *Current Drug Targets. CNS and Neurological Disorders*, *3*(4), 297–313. https://doi.org/10.2174/1568007043337193
Nilsen, J., Chen, S., Irwin, R. W., Iwamoto, S., & Brinton, R. D. (2006). Estrogen protects neuronal cells from amyloid beta-induced apoptosis via regulation of mitochondrial proteins and function. *BMC Neuroscience*, *7*(1), 74. https://doi.org/10.1186/1471-2202-7-74
Nilsen, J., & Diaz Brinton, R. (2003). Mechanism of estrogen-mediated neuroprotection: regulation of mitochondrial calcium and Bcl-2 expression. *Proceedings of the National Academy of Sciences of the United States of America*, *100*(5), 2842–2847. https://doi.org/10.1073/pnas.0438041100
Nunez, P. L., & Srinivasan, R. (2005). *Electric fields of the brain* (2nd ed.). Oxford University Press. https://doi.org/10.1093/acprof:oso/9780195050387.001.0001
Nyhus, E., & Curran, T. (2010). Functional role of gamma and theta oscillations in episodic memory. *Neuroscience and Biobehavioral Reviews*, *34*(7), 1023–1035. https://doi.org/10.1016/j.neubiorev.2009.12.014
Palacios-García, I., Silva, J., Villena-González, M., Campos-Arteaga, G., Artigas-Vergara, C., Luarte, N., Rodríguez, E., & Bosman, C. A. (2021). Increase in beta power reflects attentional top-down modulation after psychosocial stress induction. *Frontiers in Human Neuroscience*, *15*, 630813. https://doi.org/10.3389/fnhum.2021.630813
Palamoni, O. P., de Magalhães, A. C., Moriyama, L. T., de Sousa, M. V. P., & Fortunato, T. C. (2022). Monte Carlo simulations to study light propagation through the skin of different phototypes. *Tissue Optics and Photonics II*, *12147*, 28–34. https://doi.org/10.1117/12.2621670
Palva, S., & Palva, J. M. (2011). Functional roles of alpha-band phase synchronization in local and large-scale cortical networks. *Frontiers in Psychology*, *2*, 204. https://doi.org/10.3389/fpsyg.2011.00204
Pappalettera, C., Cacciotti, A., Nucci, L., Miraglia, F., Rossini, P. M., & Vecchio, F. (2023). Approximate entropy

analysis across electroencephalographic rhythmic frequency bands during physiological aging of human brain. *GeroScience*, *45*(2), 1131–1145. https://doi.org/10.1007/s11357-022-00710-4

Patergnani, S., Suski, J. M., Agnoletto, C., Bononi, A., Bonora, M., De Marchi, E., Giorgi, C., Marchi, S., Missiroli, S., Poletti, F., Rimessi, A., Duszynski, J., Wieckowski, M. R., & Pinton, P. (2011). Calcium signaling around Mitochondria Associated Membranes (MAMs). *Cell Communication and Signaling: CCS*, *9*(1), 19. https://doi.org/10.1186/1478-811X-9-19

Penberthy, W. T., & Vorwaller, C. E. (2021). Utilization of the 1064 nm wavelength in photobiomodulation: A systematic review and meta-analysis. *Journal of Lasers in Medical Sciences*, *12*(1), e86. https://doi.org/10.34172/jlms.2021.86

Pfurtscheller, G., & Lopes da Silva, F. H. (1999). Event-related EEG/MEG synchronization and desynchronization: basic principles. *Clinical Neurophysiology: Official Journal of the International Federation of Clinical Neurophysiology*, *110*(11), 1842–1857. https://doi.org/10.1016/s1388-2457(99)00141-8

Qi, X., Nizamutdinov, D., Berman, M. H., Dougal, G., Chazot, P. L., Wu, E., Stevens, A. B., Yi, S. S., & Huang, J. H. (2021). Gender differences of dementia in response to intensive self-administered Transcranial and intraocular near-infrared stimulation. *Cureus*, *13*(7), e16188. https://doi.org/10.7759/cureus.16188

Reddy, O. C., & van der Werf, Y. D. (2020). The sleeping brain: Harnessing the power of the glymphatic system through lifestyle choices. *Brain Sciences*, *10*(11), 868. https://doi.org/10.3390/brainsci10110868

R.E. Dustman, D.E. Shearer, Y. Emmerson. (n.d.). *EEG and event-related potentials in normal aging*. Retrieved May 20, 2025, from https://www.sciencedirect.com/science/article/pii/030100829390005D?via=ihub

Rettberg, J. R., Yao, J., & Brinton, R. D. (2014). Estrogen: a master regulator of bioenergetic systems in the brain and body. *Frontiers in Neuroendocrinology*, *35*(1), 8–30. https://doi.org/10.1016/j.yfrne.2013.08.001

Rossiter, H. E., Davis, E. M., Clark, E. V., Boudrias, M.-H., & Ward, N. S. (2014). Beta oscillations reflect changes in motor cortex inhibition in healthy ageing. *NeuroImage*, *91*, 360–365. https://doi.org/10.1016/j.neuroimage.2014.01.012

Sachdev, R. N. S., Gaspard, N., Gerrard, J. L., Hirsch, L. J., Spencer, D. D., & Zaveri, H. P. (2015). Delta rhythm in wakefulness: evidence from intracranial recordings in human beings. *Journal of Neurophysiology*, *114*(2), 1248–1254. https://doi.org/10.1152/jn.00249.2015

Salehpour, F., Mahmoudi, J., Kamari, F., Sadigh-Eteghad, S., Rasta, S. H., & Hamblin, M. R. (2018). Brain photobiomodulation therapy: A narrative review. *Molecular Neurobiology*, *55*(8), 6601–6636. https://doi.org/10.1007/s12035-017-08Wang52-4

Sandell, J. L., & Zhu, T. C. (2011). A review of in-vivo optical properties of human tissues and its impact on PDT. *Journal of Biophotonics*, *4*(11-12), 773–787. https://doi.org/10.1002/jbio.201100062

Spera, V., Sitnikova, T., Ward, M. J., Farzam, P., Hughes, J., Gazecki, S., Bui, E., Maiello, M., De Taboada, L., Hamblin, M. R., Franceschini, M. A., & Cassano, P. (2021). Pilot study on dose-dependent effects of transcranial photobiomodulation on brain electrical oscillations: A potential therapeutic target in Alzheimer's disease. *Journal of Alzheimer's Disease: JAD*, *83*(4), 1481–1498. https://doi.org/10.3233/JAD-210058

Stacey, J. E., Crook-Rumsey, M., Sumich, A., Howard, C. J., Crawford, T., Livne, K., Lenzoni, S., & Badham, S. (2021). Age differences in resting state EEG and their relation to eye movements and cognitive performance. *Neuropsychologia*, *157*(107887), 107887. https://doi.org/10.1016/j.neuropsychologia.2021.107887

Stirone, C., Duckles, S. P., Krause, D. N., & Procaccio, V. (2005). Estrogen increases mitochondrial efficiency and reduces oxidative stress in cerebral blood vessels. *Molecular Pharmacology*, *68*(4), 959–965. https://doi.org/10.1124/mol.105.014662

Stoler, O., Stavsky, A., Khrapunsky, Y., Melamed, I., Stutzmann, G., Gitler, D., Sekler, I., & Fleidervish, I. (2022). Frequency- and spike-timing-dependent mitochondrial Ca2+ signaling regulates the metabolic rate and synaptic efficacy in cortical neurons. *eLife*, *11*. https://doi.org/10.7554/eLife.74606

Swann, N., Tandon, N., Canolty, R., Ellmore, T. M., Mcevoy, L. K., Dreyer, S., Disano, M., & Aron, A. R. (2009). Intracranial EEG reveals time- frequency- specific role right inferior frontal gyrus primary motor cortex stopping initiated responses. *J Neurosci*, *29*, 12675–12685.

Tang, L., Jiang, H., Sun, M., & Liu, M. (2023). Pulsed transcranial photobiomodulation generates distinct beneficial neurocognitive effects compared with continuous wave transcranial light. *Lasers in Medical Science*, *38*(1), 203. https://doi.org/10.1007/s10103-023-03865-4

Tang, L., Qin, H., Lin, S., & Liu, M. (2023). Effects of pulsed red and near-infrared light on neuroblastoma cells—pilot study on frequency and duty cycle. *Photonics*, *10*(3), 315. https://doi.org/10.3390/photonics10030315

Thut, G., Miniussi, C., & Gross, J. (2012). The functional importance of rhythmic activity in the brain. *Current Biology: CB*, *22*(16), R658–R663. https://doi.org/10.1016/j.cub.2012.06.061

Van Lankveld, H., Mai, A. Q., Lim, L., Hosseinkhah, N., Cassano, P., & Jean Chen, J. (2024). Simulation-based dosimetry of transcranial and intranasal photobiomodulation of the human brain: the roles of wavelength, power density and skin colour. In *bioRxiv* (p. 2024.04.05.588330). https://doi.org/10.1101/2024.04.05.588330

Vargas, E., Barrett, D. W., Saucedo, C. L., Huang, L.-D., Abraham, J. A., Tanaka, H., Haley, A. P., & Gonzalez-Lima, F. (2017). Beneficial neurocognitive effects of transcranial laser in older adults. *Lasers in Medical Science*, *32*(5), 1153–1162. https://doi.org/10.1007/s10103-017-2221-y

Wang, X., Dmochowski, J. P., Zeng, L., Kallioniemi, E., Husain, M., Gonzalez-Lima, F., & Liu, H. (2019). Transcranial photobiomodulation with 1064-nm laser modulates brain electroencephalogram rhythms. *Neurophotonics*, *6*(2). https://doi.org/10.1117/1.NPh.6.2.025013

Wang, X., Tian, F., Soni, S. S., Gonzalez-Lima, F., & Liu, H. (2016). Interplay between up-regulation of cytochrome-c-oxidase and hemoglobin oxygenation induced by near-infrared laser. *Scientific Reports*, *6*, 30540. https://doi.org/10.1038/srep30540

Wang, Y., Huang, Y.-Y., Wang, Y., Lyu, P., & Hamblin, M. R. (2017). Photobiomodulation of human adipose-derived stem cells using 810 nm and 980 nm lasers operates via different mechanisms of action. *Biochimica et Biophysica Acta. General Subjects*, *1861*(2), 441–449. https://doi.org/10.1016/j.bbagen.2016.10.008

Wynn, S. C., Townsend, C. D., & Nyhus, E. (2023). The role of theta and gamma oscillations in item memory, source memory, and memory confidence. In *bioRxiv*. https://doi.org/10.1101/2023.10.18.562880

Yang, S.-H., Liu, R., Perez, E. J., Wen, Y., Stevens, S. M., Jr, Valencia, T., Brun-Zinkernagel, A.-M., Prokai, L., Will, Y., Dykens, J., Koulen, P., & Simpkins, J. W. (2004). Mitochondrial localization of estrogen receptor beta. *Proceedings of the National Academy of Sciences of the United States of America*, *101*(12), 4130–4135. https://doi.org/10.1073/pnas.0306948101

Yokomizo, S., Roessing, M., Morita, A., Kopp, T., Ogawa, E., Katagiri, W., Feil, S., Huang, P. L., Atochin, D. N., & Kashiwagi, S. (2022). Near-infrared II photobiomodulation augments nitric oxide bioavailability via phosphorylation of endothelial nitric oxide synthase. *FASEB Journal: Official Publication of the Federation of American Societies for Experimental Biology*, *36*(9), e22490. https://doi.org/10.1096/fj.202101890R

Zamani, A. R. N., Saberianpour, S., Geranmayeh, M. H., Bani, F., Haghighi, L., & Rahbarghazi, R. (2020). Modulatory effect of photobiomodulation on stem cell epigenetic memory: a highlight on differentiation capacity. *Lasers in Medical Science*, *35*(2), 299–306. https://doi.org/10.1007/s10103-019-02873-7

Zein, R., Selting, W., & Hamblin, M. R. (2018). Review of light parameters and photobiomodulation efficacy: dive into complexity. *Journal of Biomedical Optics*, *23*(12), 1. https://doi.org/10.1117/1.jbo.23.12.120901

Zomorrodi, R., Loheswaran, G., Pushparaj, A., & Lim, L. (2019). Pulsed Near Infrared Transcranial and Intranasal Photobiomodulation Significantly Modulates Neural Oscillations: a pilot exploratory study. *Scientific Reports*, *9*(1), 6309. https://doi.org/10.1038/s41598-019-42693-x